

1 Assessing the roles emission sources and atmospheric processes play in simulating  
2  $\delta^{15}\text{N}$  of atmospheric  $\text{NO}_x$  and  $\text{NO}_3^-$  using CMAQ (version 5.2.1) and SMOKE  
3 (version 4.6).

4  
5 *Huan Fang<sup>†</sup> and Greg Michalski<sup>‡</sup>*

6  
7 <sup>†</sup>Department of Earth, Atmospheric, and Planetary Sciences Purdue University, 550 Stadium Mall  
8 Drive, West Lafayette, IN 47907, United States

9  
10 <sup>‡</sup>Department of Chemistry, Purdue University, 560 Oval Drive, West Lafayette, IN 47907, United  
11 States

12  
13  
14 Correspondence: Huan Fang, [fang63@purdue.edu](mailto:fang63@purdue.edu)

15  
16 Keywords: isotope, nitrogen, atmospheric  $\text{NO}_x$ , atmospheric nitrate,  $\text{NO}_x$  emission sources,  
17 emission inventory, emission input dataset, atmospheric processes, disperse, mixing, transport,  
18 chemical transport model, 3D CTM, NEI, SMOKE, CMAQ

## Abstract

Nitrogen oxides ( $\text{NO}_x$  = nitric oxide (NO) + nitrogen dioxide ( $\text{NO}_2$ )) are important trace gases that affect atmospheric chemistry, air quality, and climate. Contemporary development of  $\text{NO}_x$  emissions inventories is limited by the understanding of the roles of vegetation (net  $\text{NO}_x$  source or net sink), gasoline and diesel in vehicle emissions, and the application of  $\text{NO}_x$  emission control technologies. The nitrogen stable isotope composition ( $\delta^{15}\text{N}$ ) of  $\text{NO}_x$  is an effective tool to evaluate the accuracy of the  $\text{NO}_x$  emission inventories, which are based on different assumptions. In this study, we traced the changes in  $\delta^{15}\text{N}$  values of  $\text{NO}_x$  along the “journey” of atmospheric  $\text{NO}_x$ , driven by atmospheric processes after different sources emit  $\text{NO}_x$  to the atmosphere. The  $^{15}\text{N}$  was incorporated into the emission input dataset, generated from the US EPA trace gas emission model SMOKE (Sparse Matrix Operator Kernel Emissions). Then the  $^{15}\text{N}$  incorporated emission input dataset was used to run CMAQ (the Community Multiscale Air Quality Modeling System). The simulated spatiotemporal patterns in  $\text{NO}_x$  isotopic composition for both SMOKE outputs and CMAQ outputs were compared with corresponding atmospheric measurements in West Lafayette, Indiana, USA. By enhancing  $\text{NO}_x$  deposition, we simulated the expected  $\delta^{15}\text{N}$  of  $\text{NO}_3^-$  assuming no isotope fractionation during chemical conversion or deposition. These simulations were compared to  $\delta^{15}\text{N}$  of  $\text{NO}_3^-$  in NADP sites. The results indicate the potential underestimation of emissions from soil, livestock waste, off-road vehicles, and natural gas power plants and the potential overestimation of emissions from on-road vehicles and coal-fired power plants, if only considering the difference in  $\text{NO}_x$  isotopic composition for different emission sources. The estimation of atmospheric  $\delta^{15}\text{N}(\text{NO}_x)$  using CMAQ shows better agreement (by  $\sim 3\%$ ) with observations than using SMOKE (Sparse Matrix Operator Kernel Emissions), due to the consideration of mixing, dispersion, transport, and deposition of  $\text{NO}_x$  emission from different sources.

## 1. Introduction

$\text{NO}_x$  are important trace gases that affect atmospheric chemistry, air quality, and climate ( $\text{NO}_x = \text{NO} + \text{NO}_2$ ). The main sources of tropospheric  $\text{NO}_x$  are emissions from vehicles, power plants, agriculture, livestock waste, as well as the natural by-product of nitrification and denitrification occurring in soil, and lightning (Galloway, et al., 2004). The  $\text{NO}_x$  photochemical cycle generates OH and  $\text{HO}_2$  radicals, organic peroxy radicals ( $\text{RO}_2$ ), and ozone ( $\text{O}_3$ ), which ultimately oxidize  $\text{NO}_x$  into  $\text{NO}_y$  ( $\text{NO}_y = \text{NO}_x + \text{HONO} + \text{HNO}_3 + \text{HNO}_4 + \text{N}_2\text{O}_5 + \text{other N oxides}$ ). During the photochemical processes that convert  $\text{NO}_x$  to  $\text{NO}_y$ , ground-level concentrations of  $\text{O}_3$  become elevated and secondary particles are generated. Secondary aerosols in turn affect cloud physics, enhancing the reflection of solar radiation (Schwartz, 1996) and are hazardous to human health (Lighty et al., 2000). Thus, the importance of  $\text{NO}_x$  in air quality, climate, and human and environmental health makes understanding the spatial and temporal variation in the sources of  $\text{NO}_x$  a vital scientific question.

Despite years of research, however, there are still several significant uncertainties in the  $\text{NO}_x$  budget. About 15% of global  $\text{NO}_x$  emissions, ranging from 6.6 to 21 Tg N  $\text{yr}^{-1}$ , is derived from global soil  $\text{NO}_x$  emissions yet evaluating and verifying emission rates using both laboratory and field measurements is still a challenge (Jaeglé et al., 2005; Yan et al., 2005; Stehfest and Bouwman, 2006; Hudman et al., 2012). Soil  $\text{NO}_x$  emissions vary by different biome types, meteorological conditions, and soil physicochemical properties. The application of N fertilizer also has a strong effect on soil  $\text{NO}_x$  emissions, which can dramatically increase during the first 1-2 days after N fertilizer application and can take several weeks for the emission rate to drop to pre-fertilizer levels (Ludwig et al., 2001). Furthermore, the role of vegetation, acting as a net source of atmospheric  $\text{NO}_x$  when ambient  $\text{NO}_x$  concentration is below the “compensation point”, while acting as a net sink of atmospheric  $\text{NO}_x$  when ambient  $\text{NO}_x$  concentrations are above it (Johansson, 1987; Thoene, Rennenberg & Weber, 1996; Slovik et al., 1996; Webber & Rennenberg, 1996). This significantly impacts the biotic  $\text{NO}_x$  emission inventory (Almaraz et al., 2018). Uncertainties also exist in the amount of  $\text{NO}_x$  emitted during the combustion of fossil fuels by vehicles and industry. According to Parrish (2006), the estimation of on-road vehicle  $\text{NO}_x$  emission has at least 10 to 15% uncertainty. For the mileage-based algorithm, which is used in the National Emission Inventory (NEI), the uncertainty is caused by the limited number of sites to determine the emission factors of vehicle classifications and emission types (Ingalls, 1989; Pierson et al., 1990; Fujita et al., 1992; Pierson et al., 1996; Singer and Harley, 1996). The uncertainty of the alternative fuel-based approach is caused by the fuel sales data and emission factors (Sawyer et al., 2000). The uncertainty in power plant  $\text{NO}_x$  emissions results from the choice of emission control technologies, of which the removal efficiencies of  $\text{NO}_x$  emission are different.  $\text{NO}_x$  removal by low  $\text{NO}_x$  burning, over-fire air reduction, and selective non-catalytic reduction is highly variable, ranging from 50 to 75% (Srivastava et al., 2005).

The nitrogen stable isotope composition of  $\text{NO}_x$  might be a useful tool to help resolve the uncertainties of how  $\text{NO}_x$  emission sources vary in space and time because natural and anthropogenic  $\text{NO}_x$  sources have distinctive  $^{15}\text{N}/^{14}\text{N}$  ratios (Ammann et al., 1999; Felix et al., 2012; Felix and Elliott, 2013; Fibiger et al., 2014; Heaton, 1987; Hoering, 1957; Miller et al., 2017; Walters et al., 2015a, 2015b, 2018). This variability in  $\text{NO}_x$   $^{15}\text{N}/^{14}\text{N}$  ratios is quantified by

$$\delta^{15}\text{N}(\text{NO}_x) (\text{‰}) = [({}^{15}\text{NO}_x/{}^{14}\text{NO}_x) / ({}^{15}\text{N}_2/{}^{14}\text{N}_2)_{\text{air}} - 1] \times 1000 \quad \text{Eq. (1)}$$

where  $^{15}\text{NO}_x/^{14}\text{NO}_x$  is the measurement of relative abundance of  $^{15}\text{N}$  to  $^{14}\text{N}$  in atmospheric  $\text{NO}_x$ , compared with the ratios in air  $\text{N}_2 = 0.0036$ . Previous research has shown that there are distinctive differences in  $\delta^{15}\text{N}$  values for  $\text{NO}_x$  from different emission sources and significant variations within each source (Fig. 1). Soil  $\text{NO}_x$  has the lowest  $\delta^{15}\text{N}$  values (Li & Wang, 2008; Felix & Elliott, 2014; Yu & Elliott, 2017; Miller et al., 2018) followed by waste (Felix & Elliott, 2014) and  $\text{NO}_x$  emissions from vehicles (Moore, 1977; Heaton, 1990; Ammann et al., 1999; Pearson et al., 2000; Savard et al., 2009; Redling et al., 2013; Fibiger, 2014; Felix & Elliott, 2014; Walters et al., 2015a; Walters et al., 2015b). The  $\text{NO}_x$  emissions from natural gas power plants are isotopically heavier than soil and waste (Walters et al., 2015b) while those from coal-fired power plants have the highest values (Heaton, 1987; Heaton, 1990; Snape, 2003; Felix et al., 2012; Felix et al., 2015; Savard et al., 2017). The implement of emission control technology tends to increase  $\text{NO}_x$   $\delta^{15}\text{N}$  values in both coal-fired power plants (Felix et al., 2012) and vehicles (Walters et al., 2015a). These distinctive differences in  $\delta^{15}\text{N}$  values among different  $\text{NO}_x$  emission sources suggest  $\delta^{15}\text{N}$  could be an effective tracer of atmospheric  $\text{NO}_x$  sources. For example, Redling et al. (2003) found higher  $\delta^{15}\text{N}$  of  $\text{NO}_2$  in samples collected closer to the highway compared to those adjacent to a forest, showing the emissions from vehicles were dominant near the highway. A strong positive correlation between the amount of  $\text{NO}_x$  emission from coal-fired power plants within 400 km radial area of study sites and  $\delta^{15}\text{N}(\text{NO}_3^-)$  of deposition has been demonstrated (Elliott et al., 2007; 2009). What is lacking is a systematic way of connecting  $\delta^{15}\text{N}$  values of  $\text{NO}_x$  sources, regional emissions, and data from numerous studies that measure  $\delta^{15}\text{NO}_y$  (Elliott et al., 2009; Garten, 1992; Hall et al., 2016; Occhipinti, 2008; Russell et al., 1998).

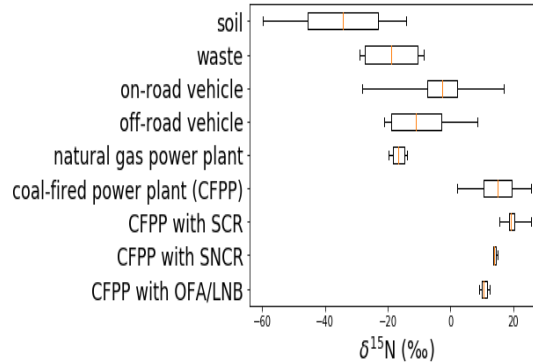


Figure 1: Box (lower quartile, median, upper quartile) and whisker (lower extreme, upper extreme) plot of the distribution of  $\delta^{15}\text{N}$  values for various  $\text{NO}_x$  emission sources.

Here we have simulated the emission of  $^{15}\text{NO}_x$  and its mixing in the atmosphere and compared the predicted  $\delta^{15}\text{N}(\text{NO}_x, \text{NO}_3^-)$  values to observations. The  $\delta^{15}\text{N}$  values of atmospheric  $\text{NO}_x$  are impacted by three main factors. The first is the inherent variability of the  $\delta^{15}\text{NO}_x$  emissions in time and space. Secondly, atmospheric processes that mix the emitted  $\text{NO}_x$ , blurring multiple emission sources within a mixing lifetime relative to the  $\text{NO}_x$  chemical lifetime (2-7 hours), which depends on its concentration and photooxidation chemistry, that also vary in time and by location (Laughner & Cohen, 2019). And thirdly, isotope effects occurring during tropospheric photochemistry may alter the  $\delta^{15}\text{NO}_x$  emissions as they are transformed from  $\text{NO}_x$  into  $\text{NO}_y$ . In this paper, we consider the effects from the first and second considerations, the temporal and spatial variation in  $\text{NO}_x$

emission and the impacts from atmospheric transport and deposition processes (source and mixing hypothesis). We accomplish this by incorporating an input dataset of  $^{15}\text{N}$  emissions used in simulations by the Chemistry-Transport Model (CTM) used in CMAQ (The Community Multiscale Air Quality Modeling System). In a companion paper, we will discuss the impacts of tropospheric photochemistry by incorporating a  $^{15}\text{N}$  chemical mechanism (Fang et al., 2021) into CMAQ. The ultimate goal will be to evaluate the accuracy of the  $\text{NO}_x$  emission inventory using  $^{15}\text{N}$ .

## 2. Methodology

### 2.1 Incorporating $^{15}\text{N}$ into $\text{NO}_x$ emission datasets

The EPA trace gas emission model SMOKE (Sparse Matrix Operator Kernel Emissions) was used to simulate  $^{14}\text{NO}_x$  and  $^{15}\text{NO}_x$  emissions.  $^{14}\text{NO}_x$  emissions were estimated using the SMOKE model based on the 2002 NEI (National Emission Inventory, USEPA, 2014), and  $^{15}\text{N}$  emissions were determined using these  $^{14}\text{NO}_x$  emissions and the corresponding  $\delta^{15}\text{N}$  values of  $\text{NO}_x$  sources from previous research (Table 1). Using the definition of  $\delta^{15}\text{N}$  (‰),  $^{15}\text{NO}_x$  emitted by each SMOKE processing category (area, biogenic, mobile, and point) was calculated by

$$^{15}\text{NO}_x(i) = ^{14}\text{NO}_x(i) \times ^{15}R_{\text{NO}_x}(i) \quad \text{Eq. (2)}$$

where  $^{14}\text{NO}_x(i)$  are the  $\text{NO}_x$  emissions for each category ( $i$ ) obtained from NEI and SMOKE and  $^{15}R_{\text{NO}_x}$  is a  $^{15}\text{N}$  emission factor ( $^{15}\text{NO}_{x(i)}/^{14}\text{NO}_{x(i)}$ ) calculated by:

$$^{15}R_{\text{NO}_x}(i) = \left( \frac{\delta^{15}\text{N}_{\text{NO}_x(i)}}{1000} + 1 \right) \times 0.0036 \quad \text{Eq. (3)}$$

$\delta^{15}\text{N}_{\text{NO}_x(i)}$  is the  $\delta^{15}\text{N}$  value of some  $\text{NO}_x$  source ( $i$  = area, biogenic, mobile, and point) and 0.0036 is the  $^{15}\text{N}/^{14}\text{N}$  of air  $\text{N}_2$ , the reference point for  $\delta^{15}\text{N}$  values.

Annual  $\text{NO}_x$  emissions for 2002 were obtained from the NEI at the county-level and were converted into hourly emissions on a 12 km x 12 km grid as previously published (Spak, Holloway, & Stone, 2007). The modeling domain includes latitudes between 37° N and 45° N, and longitudes between 98° W and 78° W, which fully covers the Midwestern US (Fig. 2, in yellow). SMOKE categorizes  $\text{NO}_x$  emissions into four “processing categories”: Biogenic, Mobile, Point, and Area (Table 1). The choice of the 2002 version of NEI is, in part, arbitrary. However, to compare the model predicted  $\delta^{15}\text{N}$  values with observations, it requires the emission inventory to be relevant to the same timeframe as the  $\delta^{15}\text{N}$  measurements of the  $\text{NO}_y$ . The data sets we compare to the model (discussed below) span from 2002 to 2009, thus the 2002 inventory is more relevant than later inventories (2014 onward). The county-level annual  $^{14}\text{NO}_x$  emission for the Midwestern US from NEI was converted to the dataset with hourly  $^{14}\text{NO}_x$  emissions. Livestock waste and off-road vehicles classified as area sources and each county was gridded evenly. Power plants are regarded as the point source and are located in grids corresponding to their latitudes and longitudes. On-road vehicles were regarded as the mobile source by SMOKE estimated by MOBILE model (see SA). The soil  $\text{NO}_x$  produced by microbial nitrification and denitrification is classified as biogenic  $\text{NO}_x$  emission and was estimated by BEIS model (see SA).

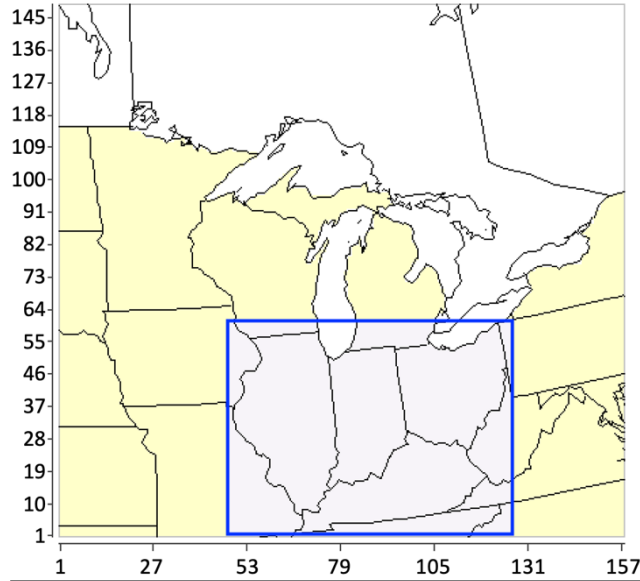


Figure 2: The full geographic domain (yellow) and extracted domain (light purple) for the study.

SMOKE Category	NEI Sector	$\delta^{15}\text{N-NO}_x$ (‰) range	$\delta^{15}\text{N-NO}_x$ (‰) this study
Biogenic	Soil	-59.8 ~ -14.0	-34.3 (Felix & Elliott, 2014)
Area	Livestock Waste	-29 ~ -8.5	-18.8 (Felix & Elliott, 2014)
	Off-road Gasoline	-21.1 ~ 8.5	-11.5 (Walters et al., 2015b)
	Off-road Diesel		-10.5 (Walters et al., 2015b)
Mobile	On-road Gasoline	-28.1 ~ 17	-2.7 (Walters et al., 2015b)
	On-road Diesel		-2.5 (Walters et al., 2015b)
Point	Coal-fired Fossil Fuel Combustion	-19.7 ~ 25.6	15 (Felix et al., 2012)
	Natural Gas Fossil Fuel Combustion		-16.5 (Walters et al., 2015)

Table 1: The  $\delta^{15}\text{N}$  values (in ‰) for  $\text{NO}_x$  emission sources based on SMOKE processing category and NEI sector

### 2.1.1 Biogenic $^{15}\text{NO}_x$ emissions

The  $\text{NO}_x$  emission from the soil (Biogenic) was modeled in SMOKE using standard techniques (details in SA) and the  $\delta^{15}\text{N}$  values of biogenic  $\text{NO}_x$  were taken from previous studies. Li & Wang (2008) measured the  $\text{NO}_x$  fluxes using dynamic flow chambers for 2 to 13 days after cropland soil was fertilized by either urea (n=9) or ammonium bicarbonate (n=9), and the  $\delta^{15}\text{N}$  values of  $\text{NO}_x$  ranged from -48.9 ‰ to -19.8 ‰. Felix & Elliott (2014) used passive samplers to collect  $\text{NO}_2$  in a cornfield for 20 days, before and after fertilizer application. The  $\delta^{15}\text{N}$  values of

NO<sub>x</sub> emissions from these measurements range from -30.8 ‰ to -26.5 ‰. Using a similar methodology, Miller et al. (2018) collected NO<sub>2</sub> between May and June finding δ<sup>15</sup>N ranging from -44.2 ‰ to -14.0 ‰ (n=37). Yu & Elliott (2017) measured -59.8 ‰ to -23.4 ‰ in 15 samples from soil plots in a fallow field 2 weeks after the precipitation. Based on these studies we adopted an average δ<sup>15</sup>N value for NO<sub>x</sub> emissions from the soil of -34.3 ‰ (Li & Wang, 2008; Felix & Elliott, 2014; Yu & Elliott, 2017; Miller et al., 2018).

#### 2.1.2 Mobile <sup>15</sup>NO<sub>x</sub> emissions

The SMOKE NO<sub>x</sub> emission from on-road vehicles used standard methods (details in SA) and used δ<sup>15</sup>N values from prior studies (Moore, 1977; Heaton, 1990; Ammann et al., 1999; Pearson et al., 2000; Savard et al., 2009; Redling et al., 2013; Felix & Elliott, 2014; Fibiger, 2014; Walters et al., 2015a, 2015b). We have excluded studies that infer NO<sub>x</sub> δ<sup>15</sup>N by measuring plant proxies or passive sampling in the environment (Ammann et al., 1999; Pearson et al., 2000; Savard et al. 2009; Redling et al., 2013; Felix & Elliott, 2014). This is because of equilibrium and kinetic isotope effects that can occur as NO<sub>x</sub> reacts in the atmosphere to form NO<sub>y</sub>, prior to NO<sub>x</sub> deposition. In addition, the role vegetation plays in NO<sub>x</sub> removal and atmospheric processes that mix the δ<sup>15</sup>N of emission with the surroundings can also alter the δ<sup>15</sup>N from the mobile source. Instead, we estimated the δ<sup>15</sup>N value of NO<sub>x</sub> emissions from vehicles only using studies that directly measured tailpipe NO<sub>x</sub> emissions. Moore (1977) and Heaton (1990) collected tailpipe NO<sub>x</sub> spanning -13 ‰ to 2 ‰, with an average of -7.5 ± 4.7 ‰. Neither Heaton nor Moore noted whether these 6 vehicles were equipped with any catalytic NO<sub>x</sub> reduction technology, but it is unlikely since the late 1970 and 80's s vehicles were seldomly equipped with catalytic NO<sub>x</sub> reduction technology. Fibiger (2014) measured 5 samples of NO<sub>x</sub> from diesel engines without SCR emitted into a smog chamber, the δ<sup>15</sup>N values range from -19.2 ‰ to -16.7 ‰ (±0.97 ‰). The most comprehensive studies on vehicle NO<sub>x</sub> δ<sup>15</sup>N values are by Walters et al. (2015a, 2015 b) who measured gas and diesel vehicles separately, including those with and without three-way catalytic converter (TCC) and SCR technology. They also measured on-road and off-road vehicles separately. This research showed that the δ<sup>15</sup>N of NO<sub>x</sub> for vehicles without SCR or when SCR was not functioning was negative, at around -15‰. As SCRs warmed and became efficient at reducing NO<sub>x</sub> the δ<sup>15</sup>N value became less negative and even went positive. The measurements showed that the δ<sup>15</sup>N values of NO<sub>x</sub> emitted by gasoline on-road vehicles averages at -2.5 ± 1.5 ‰, and on-road diesel ranged from -5 ‰ to 0 ‰.

The emission rate of <sup>15</sup>NO<sub>x</sub> from the mobile source was determined by Eq. 4 grid by grid, according to the contributions from on-road gasoline vehicles and on-road diesel vehicles, as well as their corresponding δ<sup>15</sup>N values of these two types of vehicles grid by grid. NO<sub>x</sub> emissions from off-road vehicles are regarded as area sources in SMOKE, which were processed over each county. In contrast, NO<sub>x</sub> emissions from on-road vehicles are regarded as the mobile source in SMOKE, which will be processed along each highway. Each grid emission rate of <sup>15</sup>NO<sub>x</sub> was assigned based on the contributions from gasoline and diesel vehicles, as well as the relative δ<sup>15</sup>N values. The δ<sup>15</sup>N of on-road gasoline vehicles (-2.7 ± 0.8 ‰) was based on the average of the vehicle travel time within each region with the same zip code (Walters et al., 2015b).

$$^{15}\text{NO}_x (\text{mobile}) = \left( \frac{\delta^{15}\text{N}_{\text{NO}_x (\text{on-road gas})}}{1000} + 1 \right) \times 0.0036 \times ^{14}\text{NO}_x (\text{on-road gas}) \\ + \left( \frac{\delta^{15}\text{N}_{\text{NO}_x (\text{on-road diesel})}}{1000} + 1 \right) \times 0.0036 \times ^{14}\text{NO}_x (\text{on-road diesel}) \quad \text{Eq. (4)}$$

$$\text{Where } \delta^{15}\text{N}_{\text{NO}_x (\text{on-road gas})} = -12.35 + 3.02 \times \ln(t + 0.455)$$

### 2.1.3 Point source $^{15}\text{NO}_x$ emissions

$\text{NO}_x$  point sources are large anthropogenic  $\text{NO}_x$  emitters located at a fixed, stationary position such as EGUs (electric generating units). Fugitive dust does not significantly contribute to point  $\text{NO}_x$  emissions, so our inventory focused only on power plants (Houyoux, 2005). Power plants were separated into two different types: EGU and Non-EGU (e.g. commercial and industrial combustions). The  $\delta^{15}\text{N}$  value of  $\text{NO}_x$  emitted from power plants have been estimated to vary from -19.7 ‰ to 25.6 ‰ (Heaton, 1987; Heaton, 1990; Snape, 2003; Felix et al., 2012; Felix et al., 2015; Walters et al., 2015b; Savard et al., 2017). We have ignored studies that measured  $\delta^{15}\text{N}$  of  $\text{NO}_3^-$  or  $\text{HNO}_3$  from EGUs (Felix et al., 2015, Savard et al., 2017) and instead, only consider those studies that directly measured  $\delta^{15}\text{N}$  of  $\text{NO}_x$ . Heaton (1990) collected 5 samples from the different coal-fired power stations finding  $\text{NO}_x$  from 6 ‰ to 13 ‰, with a standard deviation of 2.9 ‰. Snape (2003) measured  $\delta^{15}\text{N}$  values of 36 samples from power plants using three different types of coals in combustion chars in a drop tube reactor, with values ranging from 2.1 ‰ to 7.2 ‰, with a standard deviation of 1.37 ‰. The most comprehensive study on coal-fired power plants'  $\text{NO}_x$  values was by Felix et al. (2012). They measured the  $\delta^{15}\text{N}$  values of  $\text{NO}_x$  emission from the coal-fired power stations with and without different emission control technologies. 16 coal-fired power plants with SCR, 3 coal-fired power plants with SNCR, 15 coal-fired power plants with OFA/LNB, and 8 coal-fired power plants without emission control technology were measured. The  $\delta^{15}\text{N}$  values of  $\text{NO}_x$  emissions from these 42 measurements range from 9 ‰ to 25.6 ‰, with a standard deviation of 4.51 ‰. The  $\text{NO}_x$   $\delta^{15}\text{N}$  values when different emission control technologies were used varied: the  $\delta^{15}\text{N}$  values of  $\text{NO}_x$  emissions from coal-fired power plants with SCR range from 15.5 ‰ to 25.6 ‰, those with SNCR ranged from 13.6 ‰ to 15.1 ‰, and those with OFA/LNB ranged from 9.0 ‰ to 12.6 ‰. The  $\delta^{15}\text{N}$  values of  $\text{NO}_x$  emissions from coal-fired power plants without emission control technology range from 9.6 ‰ to 11.7 ‰, with a standard deviation of 0.79 ‰. According to Xing et al. (2013), about half of the coal-fired power plants in the United States are equipped with SCR. Thus, we assume 15 ‰ for the  $\text{NO}_x$  emissions from coal-fired power plants, which is the average between SCR and other emission control technologies.

The most comprehensive study on natural gas-fired  $\text{NO}_x$  values (Walters et al. 2015) collected 12 flue samples on the rooftop of a house from the ventilation pipe of a natural gas low- $\text{NO}_x$  burner residential furnace without  $\text{NO}_x$  emission control technology. The measurement showed that the  $\delta^{15}\text{N}$  values of  $\text{NO}_x$  emitted by natural gas power plants average  $-16.5 \pm 1.7$  ‰, which we used for the  $\text{NO}_x$  emission from natural gas power plants. The reason for using these values is because they were measurements taken directly from the exhaust pipes, rather than inferring from downwind area or from rain samples, emitted by natural gas power plants, and included power plants with and without SCR technology. The latitude, longitude, and point sources characteristics (EGU and non-EGU, coal-fired or natural gas-fired, implementation of emission control technology) of each power plant was obtained from the US Energy Information Administration (2017). The power plants were assigned grids by their latitudes and longitudes, and the  $\delta^{15}\text{N}$  values were assigned to these grids based on their emission characteristics, before determining the emission rate of  $^{15}\text{NO}_x$  from point source using Eq. (2) and (3).

### 2.1.4 Area source $^{15}\text{NO}_x$ emissions

Area  $\text{NO}_x$  (details in SA)  $\delta^{15}\text{N}$  values were based on the assumption that livestock waste and off-road vehicles (utility vehicles for agricultural and residential purposes) accounted for total area sources. Livestock waste  $\text{NO}_x$   $\delta^{15}\text{N}$  values were taken from Felix & Elliott (2014) since it is currently the only study about the  $\delta^{15}\text{N}$  value of  $\text{NO}_x$  livestock waste emissions. They placed a



passive sampler with ventilation fans in an open-air and closed room in barns of cows and turkeys, respectively. The  $\delta^{15}\text{N}$  values of  $\text{NO}_x$  emissions from these measurements range from -29 ‰ to -8.5 ‰. Among these samples, the  $\delta^{15}\text{N}$  of  $\text{NO}_x$  emissions from turkey waste averages at -8.5 ‰, the  $\delta^{15}\text{N}$  of  $\text{NO}_x$  emissions from cow waste averages at -24.7 ‰. We used -18.8 ‰ as the values of  $\delta^{15}\text{N}$  values for  $\text{NO}_x$  emissions from livestock waste, which is the weighted average of the  $\delta^{15}\text{N}$  of  $\text{NO}_x$  from turkey waste and cow waste emissions. We used the  $\delta^{15}\text{N}$  values from Walters et al. (2015b) to estimate the  $\delta^{15}\text{N}$  value of  $\text{NO}_x$  emissions from the off-road vehicle since it is the latest in-depth study that measured the  $\delta^{15}\text{N}$  value of  $\text{NO}_x$  specifically from the off-road vehicle. They collected 45 samples from the tailpipe of 9 different off-road vehicles (gasoline and diesel) with and without SCR, and before and after the sufficient engine warm-up times. The measurement showed that the  $\delta^{15}\text{N}$  values of  $\text{NO}_x$  emitted by gasoline-powered off-road vehicles averaged -11.5  $\pm$  2.7 ‰, diesel off-road vehicles without SCR averaged -19 ‰  $\pm$  2 ‰, and diesel off-road vehicles with SCR averaged -2 ‰  $\pm$  8 ‰. The emission rate of  $^{15}\text{NO}_x$  from area source was determined by Eq. 5 grid by grid, according to the contributions from waste, off-road gasoline vehicle, and off-road diesel vehicle, as well as their corresponding  $\delta^{15}\text{N}$  values based on previous researches.

$$^{15}\text{NO}_x(\text{area}) = \left( \frac{\delta^{15}\text{NNO}_x(\text{waste})}{1000} + 1 \right) \times 0.0036 \times ^{14}\text{NO}_x(\text{waste}) \\ + \left( \frac{\delta^{15}\text{NNO}_x(\text{off-road gas})}{1000} + 1 \right) \times 0.0036 \times ^{14}\text{NO}_x(\text{off-road gas}) \\ + \left( \frac{\delta^{15}\text{NNO}_x(\text{off-road diesel})}{1000} + 1 \right) \times 0.0036 \times ^{14}\text{NO}_x(\text{off-road diesel}) \quad \text{Eq. (5)}$$

The  $^{15}\text{NO}_x$  emission data files of each SMOKE processing category was incorporated into the final dataset based on the  $\delta^{15}\text{N}$  values from previous research (Table 1) and Eq. (2-5).

$$\delta^{15}\text{N}_{\text{NO}_x(\text{total})} = \left( \frac{^{15}\text{NO}_x(\text{area}) + ^{15}\text{NO}_x(\text{biog}) + ^{15}\text{NO}_x(\text{mobile}) + ^{15}\text{NO}_x(\text{point})}{^{14}\text{NO}_x(\text{area}) + ^{14}\text{NO}_x(\text{biog}) + ^{14}\text{NO}_x(\text{mobile}) + ^{14}\text{NO}_x(\text{point})} - 1 \right) \times 1000 \quad \text{Eq. (6)}$$

## 2.2 Simulating atmospheric $\delta^{15}\text{N}(\text{NO}_x)$ in CMAQ

In order to investigate the role of mixing in the spatiotemporal distribution of  $\text{NO}_x$   $\delta^{15}\text{N}$  values, CMAQ was used to simulate the meteorological transport effects (advection, eddy diffusion, etc). In this “emission + mixing” scenario grid specific  $\text{NO}_x$   $\delta^{15}\text{N}$  values emitted blur as  $\text{NO}_x$  mixes across the regional scale. This blurring will depend on grid emission strength and mixing vigor and is effectively treating  $\text{NO}_x$  as a conservative tracer. The simulations used the 2002 National Emission Inventory (NEI), as well as 2002 and 2016 meteorological conditions respectively, in order to explore how meteorological conditions will impact the atmospheric  $\delta^{15}\text{N}(\text{NO}_x)$ . Simulations covering the full domain and extracted domain were conducted, in order to explore and eliminate the bias near the domain boundary.

In addition, CMAQ simulated the  $\delta^{15}\text{NO}_x$  effect by  $\text{NO}_x$  removal using enhanced deposition. These “emission + mixing + enhanced deposition” simulations were **not** imposing an isotope effect related to dry/wet deposition, rather they are an attempt to show how “lifetime chemistry” alters  $\text{NO}_x$   $\delta^{15}\text{N}$  values by removing  $\text{NO}_x$  before it can be transported significant distances. For example, in an “emission + mixing” scenario  $\text{NO}_x$  from a high emission powerplant could travel across the domain altering regional  $\text{NO}_x$   $\delta^{15}\text{N}$  as it mixes with other grids. By contrast, in the “emission + mixing + enhanced deposition” scenario most of that  $\text{NO}_x$  would be removed near the power plant,

effectively constricting its  $\delta^{15}\text{N}$  influence. This enhanced deposition effect was simulated by disabling the chemistry module in CMAQ and enhancing the  $\text{NO}_x$  dry deposition rates (discussed in 2.2.3). This has an added advantage in that the deposited  $\text{NO}_x$   $\delta^{15}\text{N}$  should be similar to the  $\text{NO}_3^-$   $\delta^{15}\text{N}$ , which is not being generated in this model. We emphasize that in this model the isotope effects associated with the photochemical transformation of  $\text{NO}_x$  into  $\text{HNO}_3$  (and other higher N oxides) and deposition are ignored and will be addressed in the forthcoming paper.

#### 2.2.1 Meteorology input dataset

To explore the impact of atmospheric processes, the meteorology input datasets for the years 2002 and 2016 were prepared and compared. The CMAQ CTM (CCTM) used the NARR (North American Regional Reanalysis) and NAM (North American Mesoscale Forecast System) to convert the weather observations (every 3 hours for NARR, every 6 hours for NAM Analyses) into gridded meteorological elements, such as temperature, wind field, and precipitation, with the horizontal resolution of 12 km, and 34 vertical layers, with the thickness, increases with height, from 50 m near the surface to 600 m near the 50 mb pressure level. These were used to generate the gridded meteorology files on an hourly basis, using the Weather Research and Forecasting Model (WRF). To maintain consistency between the  $\text{NO}_x$  emission dataset and the meteorology, the same coordinate system, spatial domain, and grid size used in the SMOKE model were used in the WRF simulation. The WRF outputs were used to prepare the CMAQ-ready meteorology input dataset using CMAQ's MCIP (the Meteorology-Chemistry Interface Processor; see SA for details). In these emission-only simulations, the deposition of  $\text{NO}_x$  was effectively set to zero. This was accomplished by defining  $\text{YO} = ^{14}\text{NO}$  and  $\text{YO}_2 = ^{14}\text{NO}_2$  (in addition to  $\text{ZO} = ^{15}\text{NO}$  and  $\text{ZO}_2 = ^{15}\text{NO}_2$ ) and setting their VDs (deposition velocities) to 0.001 (since setting them to zero collapses the simulation) in the namelist for the gas-phase species (GC\_cb6r3\_ae6\_aq.nml).

#### 2.2.2 Initial condition and boundary condition for the simulation

The meteorological fields generated by MCIP were used as the inputs for Initial Conditions Processor (ICON) and Boundary Conditions Processor (BCON), used for running CCTM of CMAQ. The ICON program prepares the initial chemical/isotopic concentrations in each of the 3D grid cells for use in the initial time step of the CCTM simulation. The BCON program prepares the chemical/isotopic boundary condition throughout the CCTM simulation. The CMAQ default ICON and BCON for a clean atmosphere were used, which had  $\text{NO}_x < 0.25$  ppb. The  $^{15}\text{NO}_x$  were added to the outputs of ICON and BCON, with the concentration equal to  $0.0036[^{14}\text{NO}_x]$ , which assumes  $\delta^{15}\text{N} = 0$  at the initial time step and outside the domain of the simulation.

#### 2.2.3 The role of deposition and chemical transformation of $\text{NO}_x$

The deposition rates  $^{14}\text{NO}_x$  and  $^{15}\text{NO}_x$  were varied to assess their role in the spatiotemporal distribution of  $\text{NO}_x$   $\delta^{15}\text{N}$  value and to emulate photooxidation of  $\text{NO}_x$ . In these “emission + mixing + enhanced deposition” simulations, the molecular mass of Y and Z were set equal (14) to ensure no isotope effect was induced by dry deposition, since the equations for dry deposition have a mass term in the diffusion coefficient calculation. The  $^{15}\text{NO}_x/\text{NO}_x$  deposition rates were amplified by first magnifying it to 20 times normal (14 kg/hectare/yr) and testing for the change in  $\text{NO}_x$  concentration relative to the normal deposition rate. Multiple tuning trials were conducted until the e-folding time (lifetime) of  $\text{NO}_x$  in the atmosphere across the domain averaged about 1 day. This is a typical average  $\text{NO}_x$  lifetime for a combination of urban, suburban, and rural environments (Laughner & Cohen, 2019). This approach is limited since  $\text{NO}_x$  lifetime varies

depending on oxidation capacity, with urban  $\text{NO}_x$  lifetimes ( $\sim 2\text{--}11$  hours) being significantly shorter than in rural conditions (Fang et al., 2021). This limitation will be resolved once  $^{15}\text{N}$  is included in the gas and aerosol chemistry modules to future versions of CMAQ.

#### 2.2.4 The simulation over the extracted domain

As mentioned in section 2.2.4, atmospheric  $\text{NO}_x$   $\delta^{15}\text{N} = 0\text{‰}$  for initial condition and boundary condition. As a result, the bias occurs near the border of the research area, mainly under the following two circumstances. Firstly, when the air mass transports out of the research area (Fig. S1). Due to the lack of the emission dataset, Canada is considered an “emission-free zone” for this research. As a result, the atmospheric  $\text{NO}_x$  is diluted, which impacts its  $\delta^{15}\text{N}$  values, especially for those with extreme  $\delta^{15}\text{N}$  values ( $\delta^{15}\text{N} < -15\text{‰}$  or  $\delta^{15}\text{N} > 5\text{‰}$ ). Secondly, the air mass with  $\delta^{15}\text{N}(\text{NO}_x) = 0$  transports from the “emission-free zone” to the research area (Fig. S2), the atmospheric  $\delta^{15}\text{N}(\text{NO}_x)$  is flattened. Therefore, to avoid the bias near the border, the extracted domain that only covers Indiana, Illinois, Ohio, and Kentucky was determined (Fig. 2, in light purple), where the measurements of  $\delta^{15}\text{N}$  values at NADP sites are available (Mase, 2010; Riha, 2013). The boundary condition for the simulation over the extracted domain is based on the CCTM output of the full-domain simulation (BCON code available on Zenodo.org (10.5281/zenodo.4311986)).

### 3. Results and Discussion

#### 3.1 Simulated spatial variability of $\text{NO}_x$ emission rates

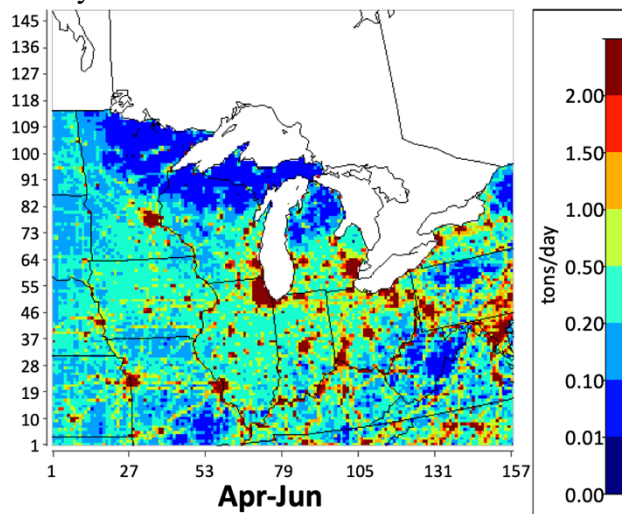


Figure 3: Total  $\text{NO}_x$  emission in the Midwest between April and June in tons/day. High  $\text{NO}_x$  emissions are associated with major urban areas such as Chicago, Detroit, Minneapolis-St Paul, Kansas City, St. Louis, Indianapolis, and Louisville.

We first examine the spatial heterogeneity of the  $\text{NO}_x$  emission rate for a single time period to illustrate the overall pattern of  $\text{NO}_x$  emission over the domain (Fig. 3). This is because the  $\delta^{15}\text{N}$  value of total  $\text{NO}_x$  emission is determined by the fraction of each  $\text{NO}_x$  source (Eq. 6), which in turn is a function of their emission rates. Since our  $\text{NO}_x$  emissions are gridded by SMOKE using the NEI, they are, by definition, corrected with respect to the NEI. However, a brief discussion of

1 the salient geographic distribution of NO<sub>x</sub> emissions and comparisons with other studies is  
2 warranted for completeness and as a backdrop for the discussion of NO<sub>x</sub> fractions and resulting  
3  $\delta^{15}\text{N}$  values. We have arbitrarily chosen to sum the NO<sub>x</sub> emissions during the April to June time  
4 period for this discussion (Fig. 3).

5 The seasonal average NO<sub>x</sub> emissions within the geographic domain during April to June range  
6 from less than 0.01 tons N/day to more than 15 tons N/day, with the seasonal grid average of 0.904  
7 tons/day. This average agrees well with estimates in previous studies for the United States, which  
8 were between 0.81 and 1.02 tons/day (Dignon & Hameed, 1989; Farrell et al., 1999; Selden et al.,  
9 1999; Xing et al, 2012). Within 75% of the geographic domain, the NO<sub>x</sub> emissions are relatively  
10 low, ranging from between 0 and 0.5 tons/day (Fig. S3). Geographically, these grids are located in  
11 rural areas some distance away from metropolitan areas and highways (Fig. 3). NO<sub>x</sub> emissions  
12 within about 20% of the grids is relatively moderate, ranging between 0.5 and 2.0 tons/day (Fig.  
13 S3). Geographically, these grids are mainly located along major highways and areas with medium  
14 population densities (Fig. 3). Urban centers comprise about 5% of the grids within the geographic  
15 domain and these have high NO<sub>x</sub> emissions rates, ranging between 2.0 and 15.0 tons/day (Fig. S3).  
16 The metropolitan area's average is 5.03 tons/day, which is nearly 14 times of the average emission  
17 rate over the rest of the grids within the geographic domain (0.37 tons/day) due to the high vehicle  
18 density associated with high population densities. The highest emissions rates are located within  
19 large cities (Fig. 3), such as Chicago, Detroit, Minneapolis-St Paul, Kansas City, St. Louis,  
20 Indianapolis, and Louisville, as well as the edge of the east coast metropolitan area (dark red).  
21 Summing the NO<sub>x</sub> emissions among the grids that encompass these major midwestern cities, yields  
22 city-level NO<sub>x</sub> emission rates that vary from 61.2 tons/day (Louisville, KY) to 634.1 tons/day  
23 (Chicago, IL). These city-level NO<sub>x</sub> emission rates (Table S4) agree well with estimates derived  
24 from the Ozone Monitoring Instrument (Lu et al., 2015). Grids containing power plants are the  
25 significant NO<sub>x</sub> hotspots within the geographic domain. These account for less than 1% of the  
26 grids, but the NO<sub>x</sub> emissions from a single grid that contains a power plant can be as high as 93.4  
27 tons/day. Geographically, the power plants are mainly located along the Ohio River valley, near  
28 other water bodies, and often close to metropolitan areas (Fig. 3). The NO<sub>x</sub> emission rates of the  
29 major power plants within the Midwest simulated by SMOKE (Table S5) match well with the  
30 measurement from the Continuous Emission Monitoring System (CEMS) (de Foy et al., 2015;  
31 Duncan et al., 2013; Kim et al., 2009). The geographic distribution of grid-level annual NO<sub>x</sub>  
32 emission density in our simulation also agrees with the county-level annual NO<sub>x</sub> emission density  
33 discussed in the 2002 NEI booklet (Fig. S4; USEPA, 2018b).

1

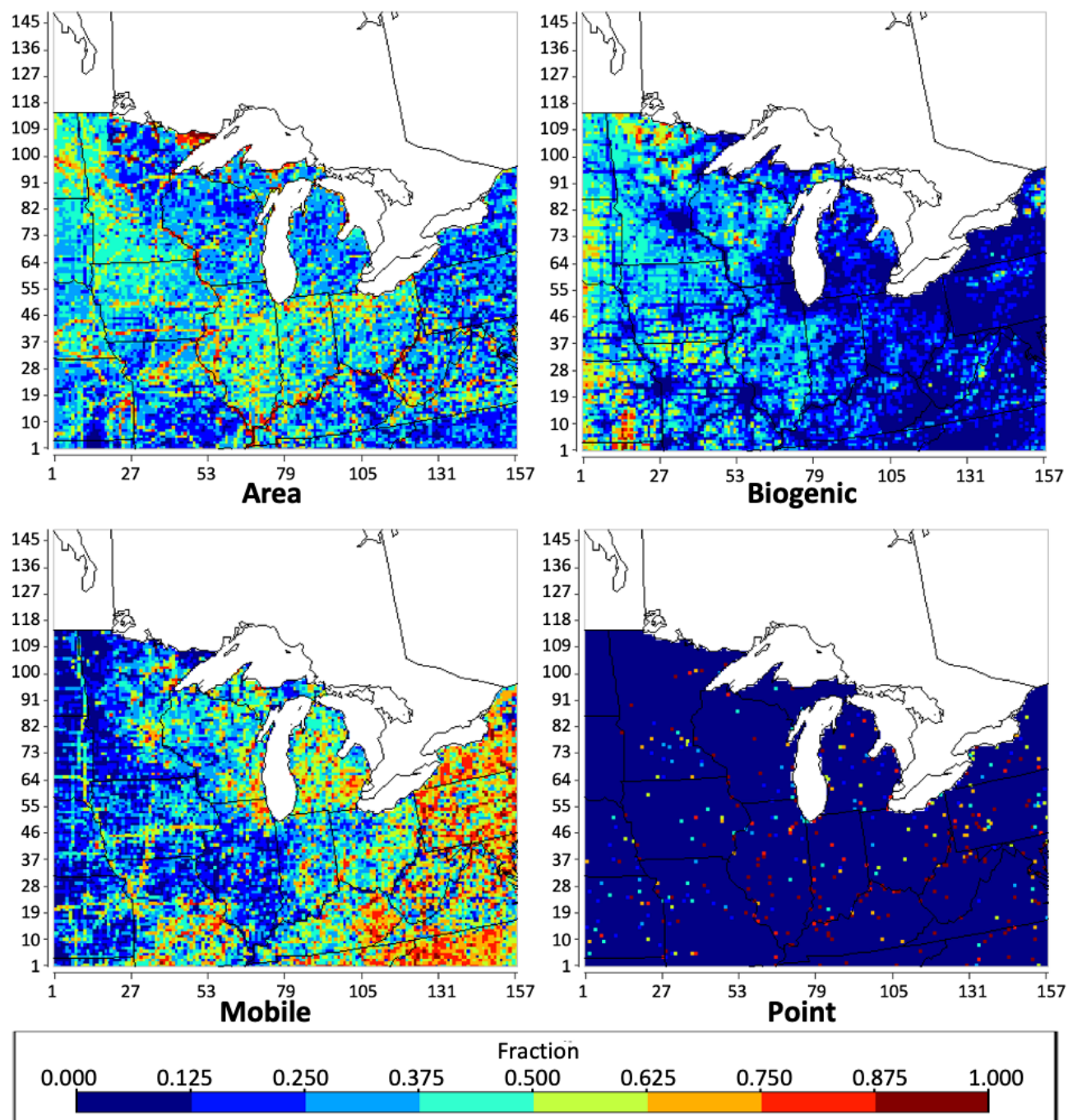


Figure 4: The geographical distribution of the fraction of  $\text{NO}_x$  emission from each SMOKE processing category (area, biogenic, mobile, point) over each grid throughout the Midwest between April and June based on NEI-2002.

2  
3  
4

1 We next examine the spatial heterogeneity of the NO<sub>x</sub> source fractions (Fig. 4) for the same  
2 time period (April to June). The NO<sub>x</sub> fraction ( $f$ ) is defined as the amount of NO<sub>x</sub> from a source  
3 category normalized to total NO<sub>x</sub> ( $f_s = \text{NO}_x(\text{source})/\text{NO}_x(\text{total})$ ). Since the  $\delta^{15}\text{NO}_x$  is determined  
4 by the NO<sub>x</sub> emission fractions within each grid it is important to understand where in the domain  
5 these fractions differ and why. The area sources, which mainly consist of off-road vehicles,  
6 agriculture production, residential combustion, as well as the industrial processes, which are  
7 individually too low in magnitude to report as point sources, are fairly uniform in their distribution  
8 across the domain.

9 The SMOKE simulation shows that NO<sub>x</sub> emissions from area sources contribute an average  
10 NO<sub>x</sub> emission fraction ( $f_{\text{area}}$ ) of 0.271 for total NO<sub>x</sub> emission and 0.290 for anthropogenic NO<sub>x</sub>  
11 emission within the Midwest from April to June. The fractions of NO<sub>x</sub> emission from area sources  
12 show a clear spatial variation and range from 0.125 to 0.5 over about 75% of the grids (Fig. S5).  
13 Geographically, the grids with relatively higher  $f_{\text{area}}$  are located in the rural area away from  
14 highways, especially in the states of Indiana, Illinois, Iowa, Minnesota, and Ohio, where  
15 agricultural is the most common land use classification. In the states of Wisconsin and Missouri,  
16 the  $f_{\text{area}}$  is slightly lower due to the higher fraction of NO<sub>x</sub> emission from biogenic sources ( $f_{\text{biog}}$ ).  
17 In the states of Pennsylvania and Michigan, the  $f_{\text{area}}$  is slightly lower due to the higher fraction of  
18 NO<sub>x</sub> emission from mobile sources ( $f_{\text{mobile}}$ ). In addition, the grids with  $f_{\text{area}}$  greater than 0.75 are  
19 mainly located along the Mississippi River and Ohio River, due to wastewater discharge.

20 The fraction of biogenic NO<sub>x</sub> ( $f_{\text{biog}}$ ) that are predominately by-products of microbial  
21 nitrification and denitrification occurring in soil, shows the clear spatial variation and is highest  
22 (from April to June) in the western portion of the domain (Fig. 4). The average fraction of biogenic  
23 NO<sub>x</sub> emission within the Midwest from April to June and is 0.065, which is less than 0.5 in more  
24 than 90% of the grids within the geographic domain (Fig. S5). Geographically, the grids with  
25 relatively high  $f_{\text{biog}}$  are located in the western regions of the Midwest, away from cities and  
26 highways, in the states of Minnesota, Iowa, Missouri, Wisconsin, and Illinois, where the density  
27 of agricultural acreage and natural vegetation is higher than other states. Furthermore, within  
28 regions with higher  $f_{\text{biog}}$ , the obvious low  $f_{\text{biog}}$  values occur in the megacities and along the  
29 highways, which agrees well with the land-use related to the biogenic emission.

30 The SMOKE simulation shows that the NO<sub>x</sub> emissions from mobile sources contribute to the  
31 fraction ( $f_{\text{mobile}}$ ) of 0.325 for total NO<sub>x</sub> emission and 0.347 for anthropogenic NO<sub>x</sub> emission within  
32 the Midwest from April to June. The  $f_{\text{mobile}}$  shows a clear spatial variation, with relatively higher  
33  $f_{\text{mobile}}$  are located in major metropolitan regions and along the highways, where vehicles have the  
34 highest density. In addition, within the states with lower  $f_{\text{mobile}}$ , the obvious high  $f_{\text{mobile}}$  values occur  
35 in the megacities and along the highways, which agrees well with the vehicle activities (US Census  
36 Bureau, n.d.). The value of  $f_{\text{mobile}}$  within the geographic domain distributes evenly on the histogram  
37 (Fig. S5).

38 The point sources consist mainly of EGUs, as well as commercial and industrial processes  
39 involving combustion. Based on the SMOKE simulation, the NO<sub>x</sub> emission from point sources  
40 contributes to the fraction ( $f_{\text{point}}$ ) of 0.339 for total NO<sub>x</sub> emission and 0.363 for anthropogenic NO<sub>x</sub>  
41 emission within the Midwest from April to June. The fractions of NO<sub>x</sub> emission from the point  
42 source over each grid cell within the geographic domain show a clear spatial variation.  
43 Geographically, the NO<sub>x</sub> emission from point sources is dominant at the grids, where the power  
44 plants are located, mainly along the Ohio River valley and near other water bodies close to  
45 metropolitan areas. The point sources have no contribution to the NO<sub>x</sub> emission among about 96%  
46 of the grids within the geographic domain. The rest of the 4% of the grids within the geographic



domain are the locations of power plants. About 1/4 of the power plants are not at the same grids as highways, thus these grids have a fraction of at least 0.9 NO<sub>x</sub> emission from point sources. Whereas the other 3/4 of the power plants share the same grids with highways/cities, thus the point sources become relatively less dominant, due to the dilution by the NO<sub>x</sub> emission from mobile sources.

### 3.2 Simulated spatial variability in $\delta^{15}\text{N}_{\text{NO}_x}$

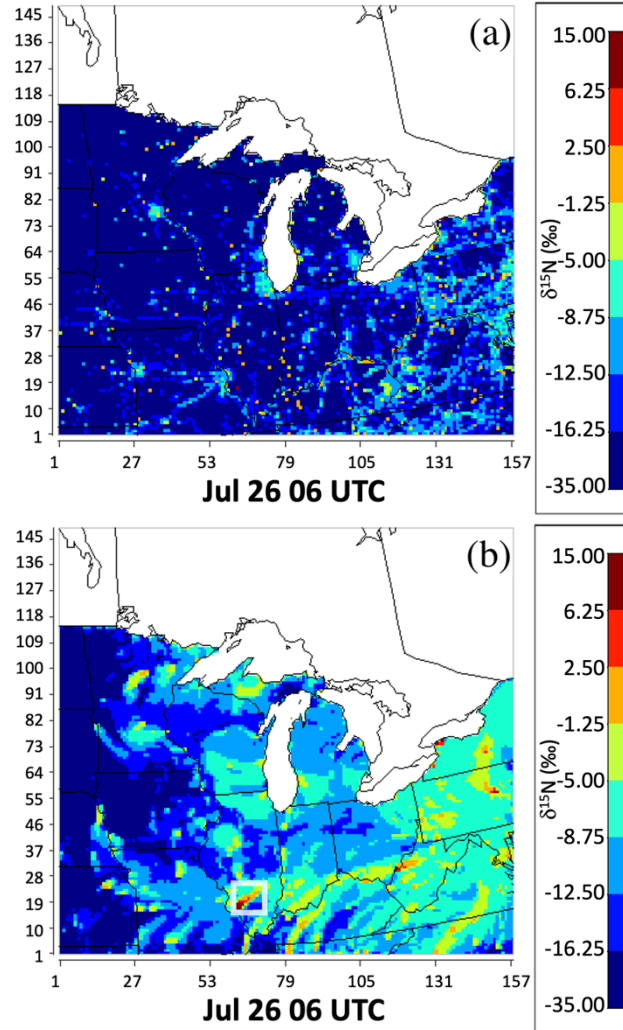


Figure 5: The  $\delta^{15}\text{N}$  values of NO<sub>x</sub> emission, (a: “no transport” scenario) and the  $\delta^{15}\text{N}$  values of atmospheric NO<sub>x</sub> based on NEI-2002 and 2016 meteorology (b: “with transport” scenario), at 06 UTC on July 26, are presented by color in each grid. The warmer the color, the higher  $\delta^{15}\text{N}$  values of atmospheric NO<sub>x</sub>.

Using these NO<sub>x</sub> emission source fractions in each grid, the  $\delta^{15}\text{N}$  values of NO<sub>x</sub> were simulated. Here, the spatial heterogeneity of  $\delta^{15}\text{N}$  values of NO<sub>x</sub> for a single time period is discussed. The “emission only” simulation of NO<sub>x</sub>  $\delta^{15}\text{N}$  values (at 06 UTC on July 26) ranged

from -34.3‰ to 14.9‰ (Fig. 5a). The majority of the grids within the domain have  $\text{NO}_x$   $\delta^{15}\text{N}$  values lower than -16.3‰. These low  $\delta^{15}\text{N}$  values across most of the domain are due to the  $\delta^{15}\text{N}$  of -34.3‰ for biogenic  $\text{NO}_x$  emission sources in sparsely populated areas where intensive agriculture dominates the land use (Fig. 5a). The  $\text{NO}_x$   $\delta^{15}\text{N}$  values for grids within big cities mainly ranged between -8.75‰ and -5‰ due to the higher fraction of  $\text{NO}_x$  emission from on-road vehicles ( $\delta^{15}\text{N} = -2.7 \pm 0.8$ ‰), which also resolve major highways. The highest value of  $\delta^{15}\text{N}$  occurs at the grids, where the coal-fired EGUs (+15‰) and hybrid-fired EGUs are the dominant  $\text{NO}_x$  source (Fig. 5a).

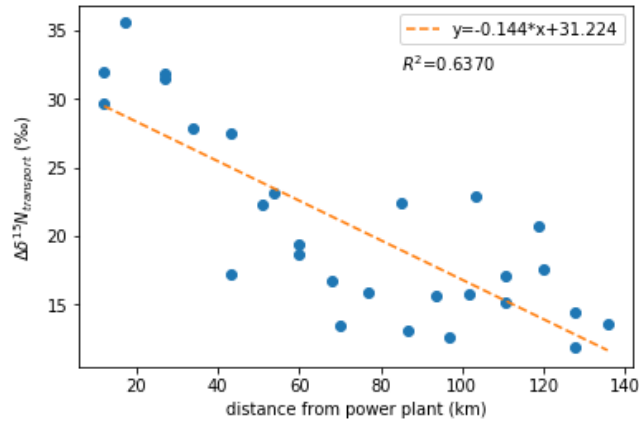


Figure 6: The  $\Delta\delta^{15}\text{N}_{\text{transport}}$  along the plume (colored in dark red to orange inside the white box on Fig. 5b) over the distance from the power plant Baldwin Energy Complex (located at southwestern border of Illinois).

The effect of atmospheric mixing on the  $\delta^{15}\text{NO}_x$  spatial distribution was then taken into account by coupling the  $^{15}\text{NO}_x$  emissions to the meteorology simulation. There are significant differences between  $\delta^{15}\text{NO}_x$  values in the “emission only” (Fig. 5a) and the “emission + transport” (Fig. 5b) simulations. For example, under the “emission only” scenario (Fig. 5a) the map of  $\delta^{15}\text{NO}_x$  values clearly shows the locations of big cities, major highways, and power plants, but these features are much less obvious in the “emission + transport” (Fig. 5b) simulations. The isotopically heavier  $\text{NO}_x$  emission from big cities disperses to the surrounding rural areas so that the  $\delta^{15}\text{NO}_x$  values in rural areas become elevated relative to the emission-only simulation. Similarly, the  $\text{NO}_x$  emitted along major highways is transported to the surrounding grids, so that the atmospheric  $\text{NO}_x$  at the grids around the major highways becomes isotopically heavier relative to the “emission only” scenario. We define  $\Delta\delta^{15}\text{N}_{\text{transport}}$  as the  $\delta^{15}\text{N}$  difference between “emission only” and “emission + transport” scenarios within the grids covered by the plume to quantify this effect (Fig. 6). The most obvious and interesting example is the influence of grids containing coal-fired EGUs on the surrounding region. For example, the southern Illinois’ Baldwin Energy Complex (marked with a transparent white box on Fig. 5b) that uses subbituminous coal and bituminous coal as its major energy source. The  $\Delta\delta^{15}\text{N}_{\text{transport}}$  in the regions is altered as a function of distance away from the EGU. In this time snapshot (06 UTC on Jul 26), the northeastwards propagating plume of  $\text{NO}_x$  emission from the EGU creates higher  $\delta^{15}\text{NO}_x$  over 135 km away (Fig. 6). The domain average  $\delta^{15}\text{N}$  increases from -20.2‰ under the “emission only” scenario to -11.5‰ under the “emission + transport” scenario. While “emission only”  $\delta^{15}\text{N}$  pattern shows biogenic emission dominating the



spatial domain, in the “emission + transport” simulation anthropogenic emissions, becomes dominant over most of the grids, especially for the grids located around major cities' power plants.

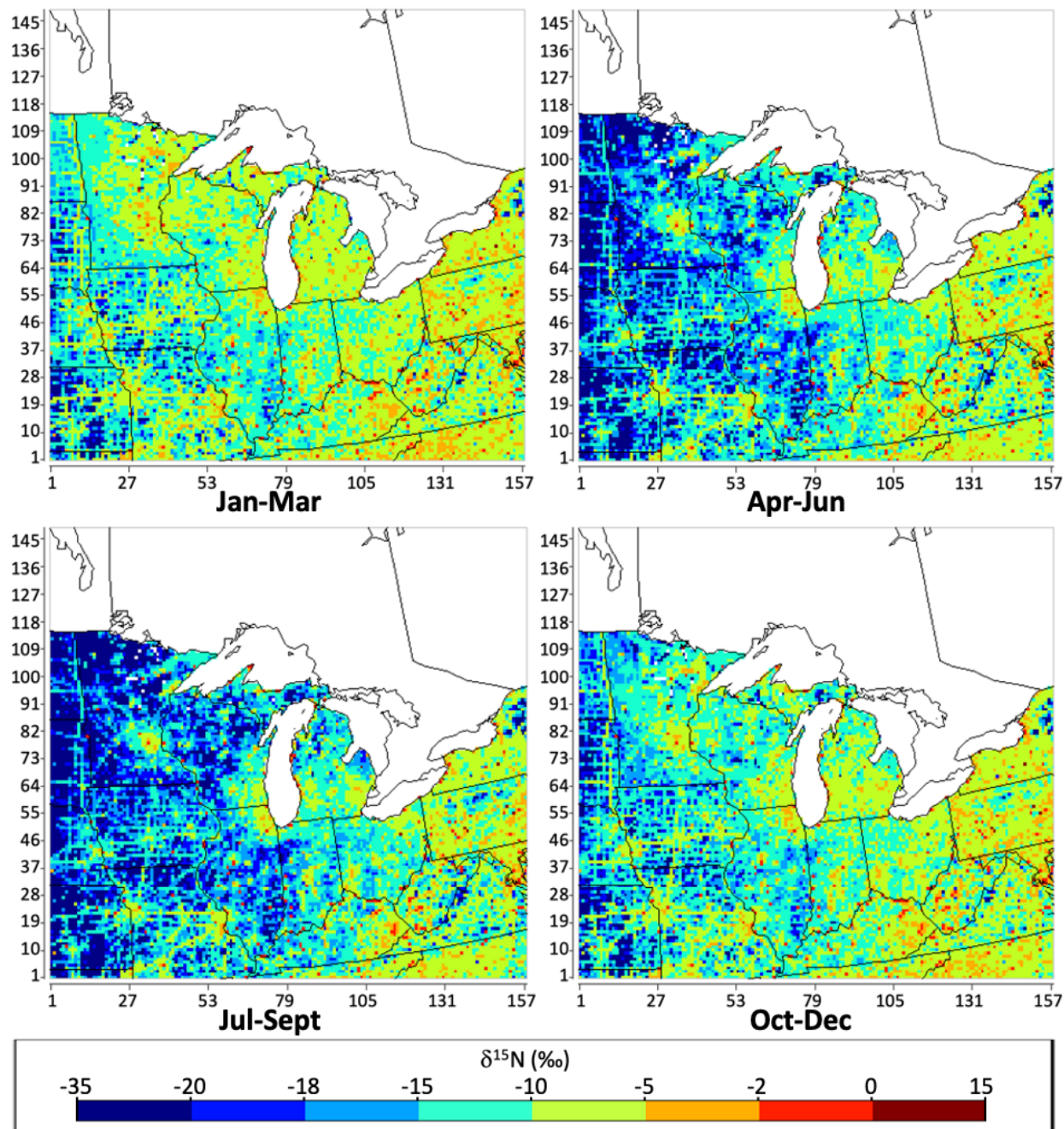


Figure 7: The geographical distribution of the  $\delta^{15}\text{N}$  value of total  $\text{NO}_x$  emissions in each season (Winter: Jan-Mar; Spring: Apr-Jun; Summer: Jul-Sep; Fall: Oct-Dec) in per mil (‰) throughout the Midwest simulated by SMOKE, based on NEI-2002.

### 3.3 Seasonal variation in $\delta^{15}\text{NO}_x$

We next examine the temporal heterogeneity of  $\delta^{15}\text{NO}_x$  values over the domain for “emission only) and interpret them in terms of changes in  $\text{NO}_x$  emission fractions as a function of time. The predicted  $\delta^{15}\text{N}$  value of total  $\text{NO}_x$  emissions in the Midwest during each season shows a significant temporal variation (Fig. 7). The  $\delta^{15}\text{NO}_x$  ranged from -35 ‰ to 15 ‰, with the annual average over the Midwest at -6.15 ‰. The maps for different seasons show the obvious changes in  $\delta^{15}\text{N}$  values over western regions of the Midwest, from green ( $\delta^{15}\text{N} = -15 \sim -5$  ‰) to dark blue (-35 ~ -15 ‰) during the month from April to October.

In order to qualitatively analyze the changes in  $\delta^{15}\text{NO}_x$  among each season, the value of each grid (Fig. 7) were organized into the histograms (Fig. S6), in order to show the percentage of the grid in each color scheme. The grids with  $\delta^{15}\text{NO}_x$  between -35‰ and -18‰ increase dramatically from less than 10% during fall (Oct-Dec) and winter (Jan-Mar) to more than 20% during spring (Apr-Jun) and summer (Jul-Sep). The grids with  $\delta^{15}\text{NO}_x$  between -18‰ and -2‰ decrease from around 90% during fall and winter to around 75% during spring and summer. In addition, the distribution of  $\delta^{15}\text{NO}_x$  shifts to lower values during spring and summer.

The significant temporal variation in the  $\delta^{15}\text{N}$  value of total  $\text{NO}_x$  during different seasons can be quantitatively explained by changing fractions of  $\text{NO}_x$  emission from the biogenic source in any grid (Fig. S7) using Eq. (6). Unlike other  $\text{NO}_x$  emission sources, the fraction of  $\text{NO}_x$  emission from biogenic sources changes significantly among each season within the geographic domain, especially over the rural areas of the states of Minnesota, Iowa, Missouri, Wisconsin, Illinois, Indiana, Kentucky, Michigan, and Ohio (Fig. S7). The fraction of  $\text{NO}_x$  emission from biogenic sources over these areas increases from less than 0.25 to more than 0.50 during the months of April to October, which is the growing season. During this period, the surface sunlight hours, temperature, and precipitation are relatively higher and as a result, the canopy coverage of the plants becomes higher, which leads to the increase of the  $\text{NO}_x$  emission from biogenic sources (Pierce, 2001; Vukovich & Pierce, 2002; Schwede et al., 2005; Pouliot & Pierce, 2009; USEPA, 2018a). Besides this, the fertilizer application during this period is also responsible for the increase in soil  $\text{NO}_x$  emission (Li & Wang, 2008; Felix & Elliott, 2014).

In order to qualitatively analyze the changes in the fraction of  $\text{NO}_x$  emission from biogenic sources among each season, the distributions of the fractions among the same cut-offs as the maps on Fig. S7 were shown in the histograms (Fig. S8). Comparing the distributions of the fractions of  $\text{NO}_x$  emission from biogenic sources among the histograms for each season, the effects from the increasing of biogenic  $\text{NO}_x$  emission during the growing season of plants are clearly shown. In general, the distribution of the fraction shifts to higher values during spring (Apr-Jun) and summer (Jul-Sep), indicating the increase of biogenic emissions. As a result, the distribution of  $\delta^{15}\text{NO}_x$  shifts to lower values during the same period (Fig. 7). The percentage of the grids with the fraction of biogenic emission less than 0.125 decreases dramatically from more than 50% during fall (Oct-Dec) and winter (Jan-Mar) to less than 35% during spring (Apr-Jun) and summer (Jul-Sep). As the  $\text{NO}_x$  emission from biogenic source becomes dominant, the percentage of the grids with  $\delta^{15}\text{NO}_x$  between -35‰ and -18‰ increases, while the percentage of the grids with  $\delta^{15}\text{N}(\text{NO}_x)$  between -18‰ and -2‰ decreases, which sufficiently explains the trends shown on Fig. 7.

1 We then examine the temporal heterogeneity of atmospheric  $\delta^{15}\text{NO}_x$  under the “emission +  
2 transport” scenario over the domain and interpret them in terms of changes in the propagation of  
3  $\text{NO}_x$  emission as a function of time. The predicted seasonal average  $\delta^{15}\text{NO}_x$  in the Midwest shows  
4 significant variations (Fig. 8). On an annual basis, the  $\delta^{15}\text{NO}_x$  values range from -19.2‰ to 11.6‰,  
5 with the annual average over the Midwest domain of -6.10‰. Compared with the seasonal  $\delta^{15}\text{NO}_x$   
6 under the “no transport” scenario, the  $\delta^{15}\text{NO}_x$  under the “with transport” scenario has a similar  
7 overall average while narrower range, due to the transport and mixing of the air mass. This could  
8 be clearly shown on the map, of which the color scheme is smoother, comparing with the seasonal  
9  $\delta^{15}\text{N}(\text{NO}_x)$  under the “no transport” scenario (Fig. 7). The maps for different seasons show the  
10 obvious changes in  $\delta^{15}\text{N}$  values over western regions of the Midwest, from -8.75 ~ -5‰ in Oct-  
11 Mar to -16.25 ~ -12.5‰ in Apr-Oct.

12 In addition to the variability of the  $\text{NO}_x$  emission source, the significant temporal variation in  
13 the  $\delta^{15}\text{N}$  value of atmospheric  $\text{NO}_x$  during different seasons is controlled by the transport and  
14 mixing of the air mass, under the different meteorology conditions that vary by season. The PBL  
15 height is an effective indicator showing whether the pollutants are under the synoptic condition,  
16 which is favorable for the dispersion, mixing, and transport after being emitted into the atmosphere  
17 (Oke, 2002; Shu et al., 2017; Liao et al., 2018; Miao et al., 2019). In order to qualitatively analyze  
18 the changes in  $\delta^{15}\text{N}$  values driven by atmospheric processes, the difference between the  $\delta^{15}\text{N}$  value  
19 of atmospheric  $\text{NO}_x$  under the “emission + transport” scenario and “emission only” scenario  
20 ( $\Delta\delta^{15}\text{N}_{\text{transport}}$ ) on the seasonal basis were shown (Fig. S9). The seasonal  $\Delta\delta^{15}\text{N}_{\text{transport}}$  values range  
21 from -21.9‰ to 31.2‰, with an average of 4.9‰. The overall pattern of the  $\Delta\delta^{15}\text{N}_{\text{transport}}$  values  
22 shows that after the  $\text{NO}_x$  being emitted into the atmosphere, it became isotopically heavier over  
23 the majority of the grids within the domain, and isotopically lighter over the grids that contain big  
24 cities, major highways, and power plants. This could be explained by the transport and dispersion  
25 of biogenic emissions and anthropogenic emission to the surrounding areas. Among the grids  
26 located in rural areas, where the biogenic emission dominates the  $\text{NO}_x$  budget, the  $\delta^{15}\text{N}$  values  
27 increases from around -30‰ to around -10‰, due to transport and dispersion of anthropogenic  
28 emission with relatively high emission rates from surrounding cities, highways, or power plants,  
29 which brings the isotopically heavier  $\text{NO}_x$  into the grids. On the other hand, among the grids  
30 located in the urban area, highways, or power plants, where anthropogenic emission dominates the  
31  $\text{NO}_x$  budget, the changes in  $\delta^{15}\text{N}$  values decrease is much less obvious, showing the  $\Delta\delta^{15}\text{N}_{\text{transport}}$   
32 values ranges between -5‰ and +5‰. This could be explained by the relatively high rates of  
33 anthropogenic emissions. Thus, the effects of the transport and dispersion of biogenic emissions  
34 from the surrounding rural area are minimal.

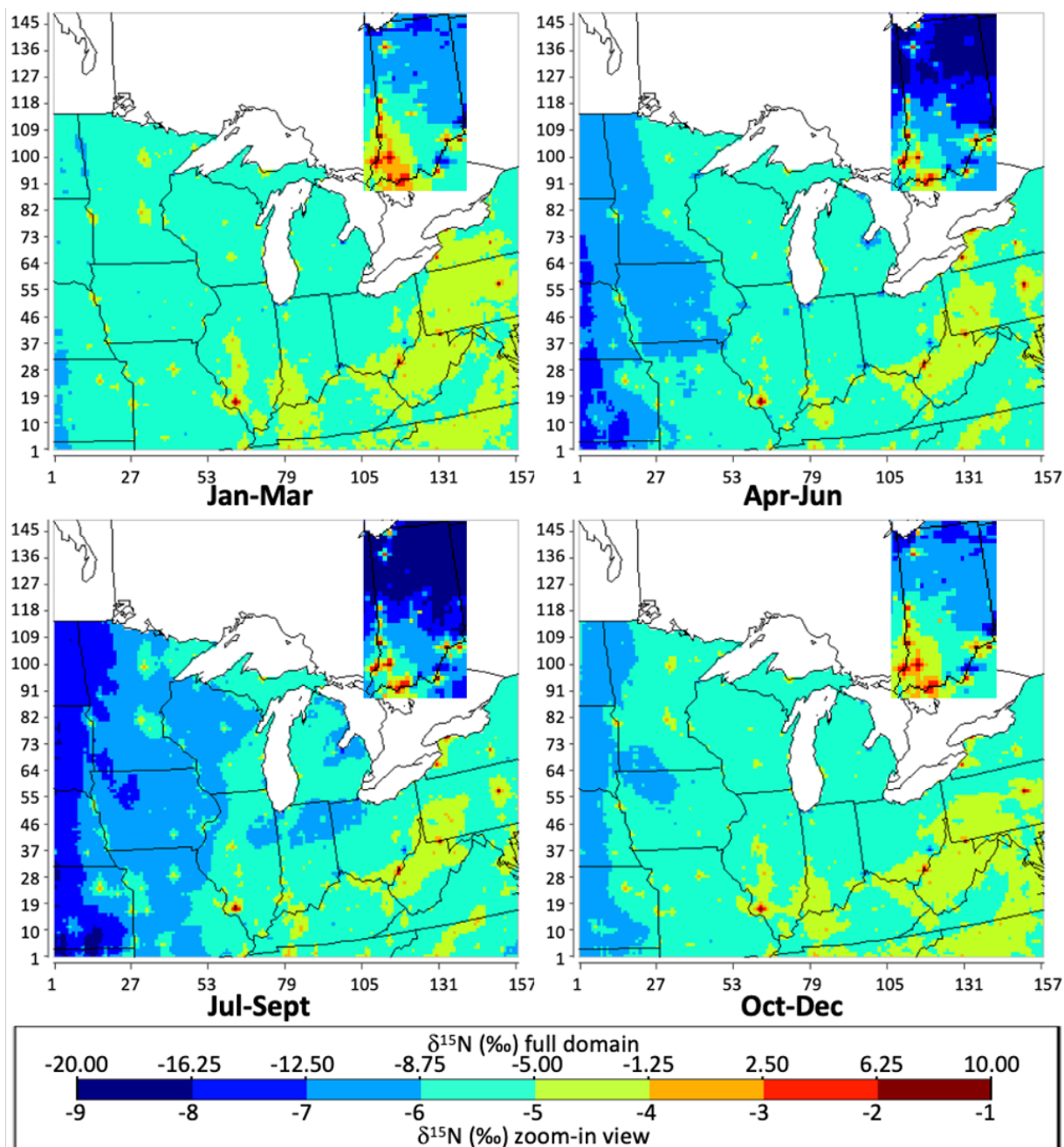


Figure 8: The geographical distribution of the  $\delta^{15}\text{N}$  value of atmospheric  $\text{NO}_x$  in each season (Winter: Jan-Mar; Spring: Apr-Jun; Summer: Jul-Sep; Fall: Oct-Dec) in per mil (‰) throughout the Midwest (with zoom-in view focusing on Indiana) simulated by CMAQ, based on NEI-2002 and 2016 meteorology.

Comparing the distributions of the difference in  $\delta^{15}\text{N}$  values (Fig. S9) with the corresponding PBL height (Fig. S10) among the maps of each season, the effects of PBL height on the propagation of the air mass are clearly shown. The PBL height changes significantly among each season within the geographic domain, especially over Minnesota, Wisconsin, and Iowa (Fig. S10). The PBL height over these areas increases from less than 250 meters above the

ground level to more than 625 meters above the ground level, during spring (Apr-Jun) and summer (Jul-Sep), which creates a more favorable synoptic condition for the dispersion, mixing, and transport of the pollutants after being emitted into the atmosphere. As a result, the difference in  $\delta^{15}\text{N}$  values shifts to higher values, showing the stronger effect of atmospheric processes during spring and summer. In order to qualitatively analyze how PBL height affects the level of the dispersion, mixing, and transport of the pollutants, the average  $\delta^{15}\text{N}$  value of atmospheric  $\text{NO}_x$  along the plumes of power plants was compared with the domain average PBL height for each month within the Midwest region. The time series plot (Fig. 9a) shows the same seasonal trend of  $\delta^{15}\text{N}$  values along the power plants plumes and PBL heights over the domain. Interestingly, the “turning point” of the  $\delta^{15}\text{N}$  values is about one month later than the “turning point” of the PBL heights. The scatter plot (Fig. 9b) shows a strong positive correlation between the domain average PBL height and average  $\delta^{15}\text{N}$  value along the power plants plumes, with  $R^2=0.85$ . The positive correlation between PBL height and propagation of air mass, indicated by the evolution of atmospheric  $\delta^{15}\text{NO}_x$  in this study, agrees well with the corresponding measurement in megacities in China from the previous studies (Shu et al., 2017; Liu et al., 2018; Liao et al., 2018).

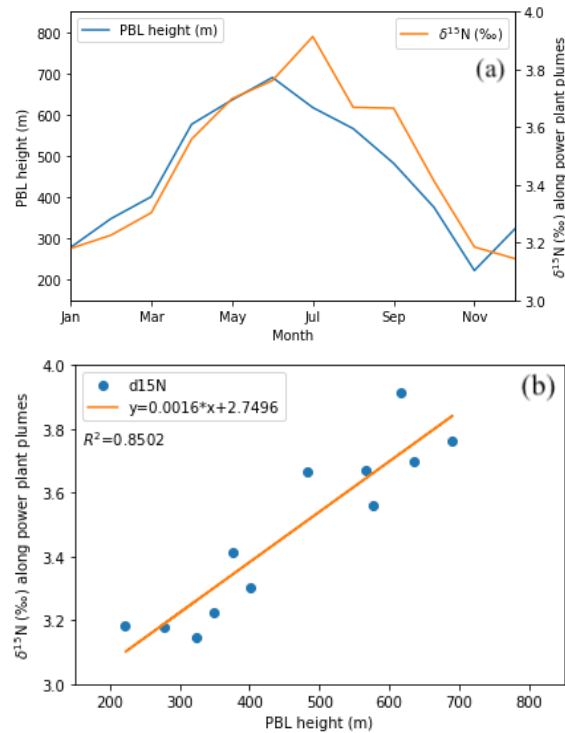


Figure 9: The time series plot (a) and the scatter plot (b) of the domain average PBL height (m) and the average  $\delta^{15}\text{N}$  (‰) value of atmospheric  $\text{NO}_x$  along the plumes of power plants during each month throughout the Midwest simulated by CMAQ, based on NEI-2002 and 2016 meteorology.

The atmospheric  $\delta^{15}\text{NO}_x$  simulated based on different meteorology input dataset varies. In order to compare the spatial heterogeneity of the atmospheric  $\delta^{15}\text{NO}_x$  under different meteorology conditions, the same analysis was done on the simulation using 2002 meteorology (Fig. S12).



Overall, the simulated atmospheric  $\text{NO}_x$  under 2002 meteorology has the similar geographic distribution and seasonal trend as the 2016 simulation. In order to qualitatively compare the propagations of the pollutants under the impact of PBL height, the same plots were generated for simulation based on 2002 meteorology (Fig. 10). Comparing to the two simulations (Fig. 10a) reveals a similar seasonal trend but stronger monthly variation. Starting with lower PBL height during the winter, the corresponding  $\delta^{15}\text{N}$  values along the power plants' plumes were lower, comparing to the simulation based on 2016 meteorology. As a result, the  $\delta^{15}\text{N}$  values during the spring and summer were also relatively lower. On the other hand, due to the higher PBL height during the spring and summer for the simulation based on 2002 meteorology, the  $\delta^{15}\text{N}$  values decreased slower since July, ending with the relatively higher  $\delta^{15}\text{N}$  values in December. The scatter plot for the simulation based on 2002 meteorology (Fig. 10b) also shows a strong positive correlation between the domain average PBL height and average  $\delta^{15}\text{N}$  value along the power plants plumes, with  $R^2=0.78$ . The videos of atmospheric  $\delta^{15}\text{NO}_x$  on an hourly basis throughout the years 2002 and 2016 are available on Zenodo.org (10.5281/zenodo.4311986).

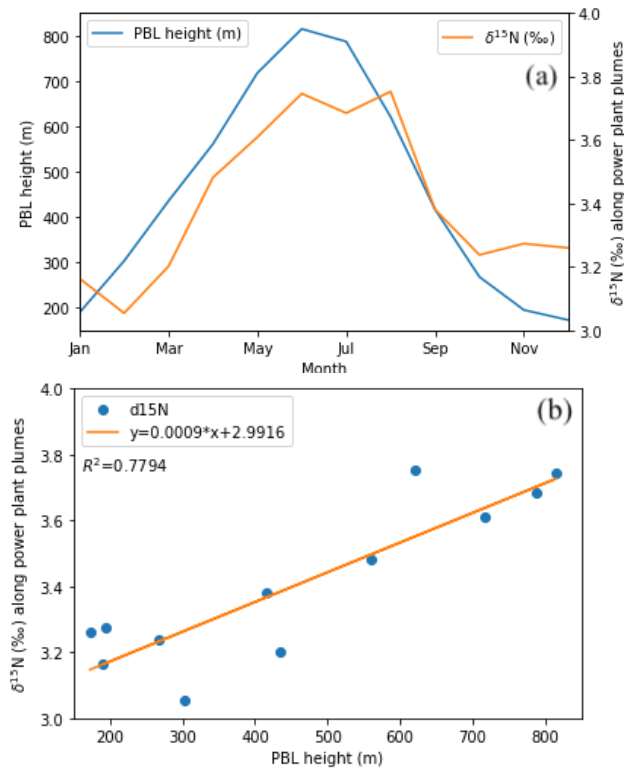


Figure 10: The time series plot (a) and the scatter plot (b) of the domain average PBL height (m) and the average  $\delta^{15}\text{N}$  (‰) value of atmospheric  $\text{NO}_x$  along the plumes of power plants during each month throughout the Midwest simulated by CMAQ, based on NEI-2002 and 2002 meteorology.

### 3.4 The simulation over the extracted domain

The temporal heterogeneity of difference in atmospheric  $\delta^{15}\text{NO}_x$  between extracted-domain simulation and full-domain simulation ( $\Delta\delta^{15}\text{N}_{\text{extracted-full}}$ ), to explore the potential bias due to the motion of the air mass across the boundary of the geographic domain of the study (Fig. 11). The

1 extracted domain covers the states of Indiana, Illinois, Ohio, and Kentucky, where the  
2 measurements of  $\delta^{15}\text{NO}_3^-$  at NADP sites are available. The predicted  $\delta^{15}\text{N}$  of atmospheric  $\text{NO}_x$   
3 over the extracted domain shows a similar overall pattern as the  $\delta^{15}\text{N}$  within the same domain from  
4 the full-domain simulation, except over the southern border of the domain (Fig. S14). In order to  
5 qualitatively analyze the effects from the initial boundary condition, the  $\delta^{15}\text{N}$  of atmospheric  $\text{NO}_x$   
6 within IN, IL, OH, and KY were extracted from the full-domain simulation (Fig. 8) and compared  
7 with the extracted-domain simulation within the same region (Fig. 11). The  $\Delta\delta^{15}\text{N}_{\text{extracted-full}}$  values  
8 ranged between  $-0.25\text{‰}$  and  $+0.25\text{‰}$  over most of the grids within the extracted domain, showing  
9 the difference between extracted-domain simulation and full-domain simulation of  $\delta^{15}\text{N}$  values are  
10 trivial. However, near the southern border of the extracted domain, the obvious  $\Delta\delta^{15}\text{N}_{\text{extracted-full}}$   
11 values close to  $+0.75\text{‰}$  during fall and winter, close to  $+1.00\text{‰}$  during spring and summer occur,  
12 which indicate the atmospheric  $\text{NO}_x$  from the extracted-domain simulation is isotopically heavier.  
13 The values of  $\Delta\delta^{15}\text{N}_{\text{extracted-full}}$  become obvious near the southern border, which indicates the  
14 dilution of  $\text{NO}_x$ , after it transports out of the domain since the  $\delta^{15}\text{N}$  on the boundary was set to  
15 zero. Unlike the southern border, the northern, western, and eastern border of the extracted domain  
16 is located a sufficient distance apart from the boundary of the full domain. As a result, the  
17  $\Delta\delta^{15}\text{N}_{\text{extracted-full}}$  values are similar over the majority grids within the domain.

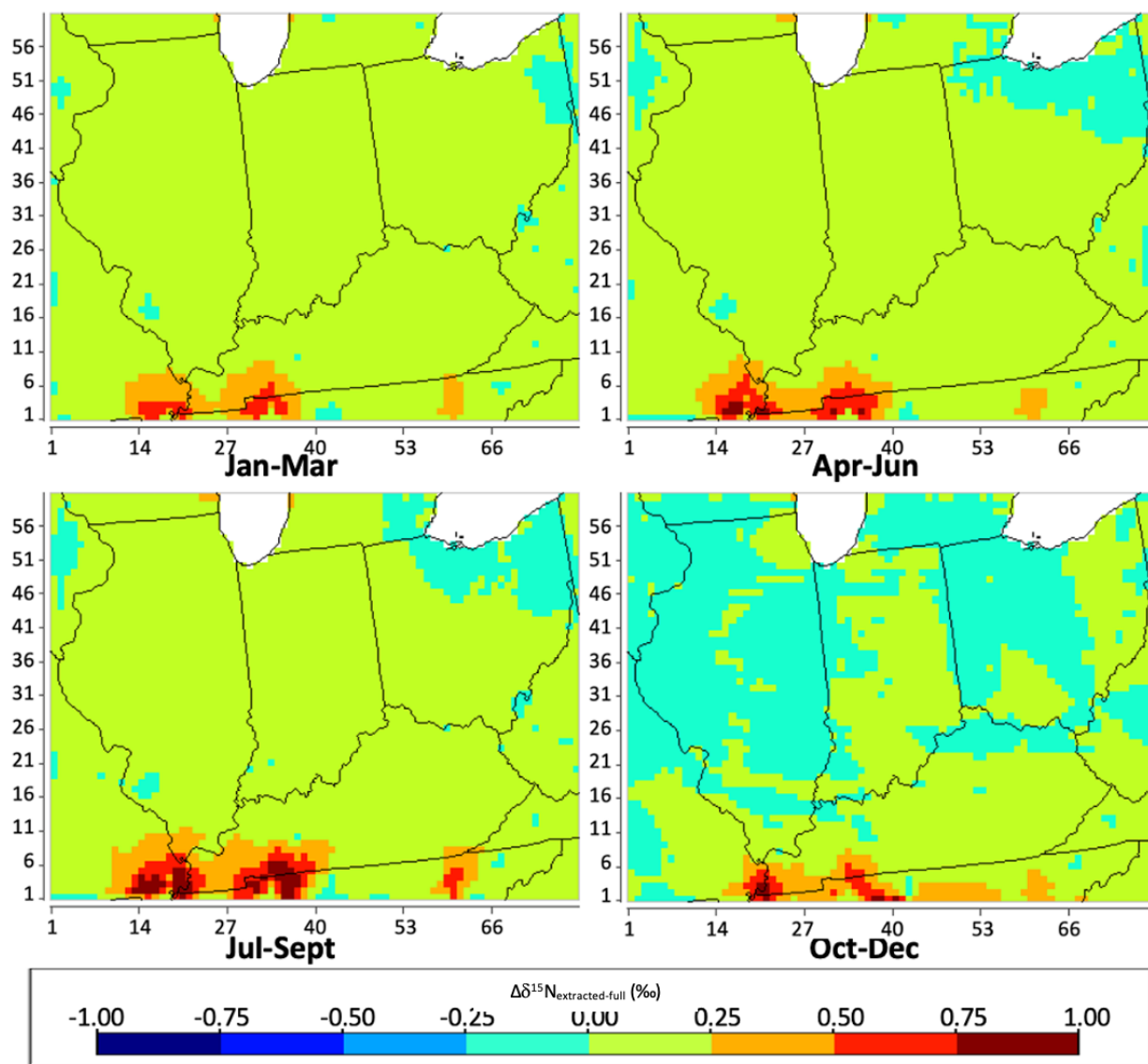


Figure 11: The geographical distribution of the difference between extracted-domain simulation and full-domain simulation of  $\delta^{15}\text{N}$  value of atmospheric  $\text{NO}_x$  ( $\Delta\delta^{15}\text{N}_{\text{extracted-full}}$ ) in each season (Winter: Jan-Mar; Spring: Apr-Jun; Summer: Jul-Sep; Fall: Oct-Dec) in per mil (‰) within IN, IL, OH, and KY, based on NEI-2002 and 2016 meteorology.

### 3.5 The role of enhanced $\text{NO}_x$ deposition



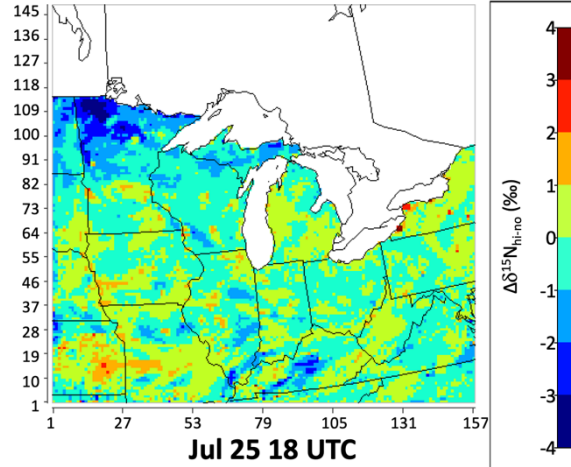


Figure 12. The  $\Delta\delta^{15}\text{N}_{\text{hi-no}}$  values at 18 UTC on July 25.

The “emission + mixing + enhanced deposition” simulations significantly alter the  $\delta^{15}\text{N}$  of atmospheric  $\text{NO}_x$  relative to the normal deposition scenarios. Again, the enhanced deposition cases are removing  $\text{NO}_x$  at rates that would be similar to those by removal during its conversion into  $\text{HNO}_3$ . Thus, in these cases the  $\text{NO}_x$  deposited is  $\sim \delta^{15}\text{NO}_3^-$  and the  $\delta^{15}\text{NO}_x$  is that in the residual  $\text{NO}_x$ . The impact of high deposition on the residual  $\text{NO}_x$  was assessed using  $\Delta\delta^{15}\text{N}_{\text{hi-no}}$ , the difference between the  $\delta^{15}\text{NO}_x$  values of atmospheric under the “enhanced deposition” and “no deposition” scenarios. The  $\Delta\delta^{15}\text{N}_{\text{hi-no}}$  range was  $\pm 4\text{‰}$  and was especially obvious downwind of the locations with large emission rates, such as power plants or megacities (Fig. 12a). This can be explained as a similar fashion to the “no deposition” scenarios (Fig. S15a), where the dispersion of the isotopically heavier  $\text{NO}_x$  emission from big cities, major highways, and power plants elevates the  $\delta^{15}\text{NO}_x$  values in the surrounding grids located in rural areas, the dispersion of the isotopically lighter biogenic  $\text{NO}_x$  emission lowers the  $\delta^{15}\text{NO}_x$  values in the surrounding grids located in the suburb of major cities (Fig. S15b). On the other hand, due to the higher deposition rate, the transport, mixing, and dispersion of  $\text{NO}_x$  emission from different sources are restricted within a smaller geographical extent (Fig. S15b). As a result, under the “enhanced deposition” scenario, the  $\text{NO}_x$  emissions disperse to fewer surrounding grids but lead to a lower  $\delta^{15}\text{NO}_x$  values relative to no deposition. The temporal heterogeneity of  $\Delta\delta^{15}\text{N}_{\text{hi-no}}$  over the domain was examined and the impact of enhancing deposition rates of  $\text{NO}_x$  on the  $\delta^{15}\text{N}$  of atmospheric  $\text{NO}_x$  on the seasonal basis was explored (Fig. 14). The seasonal  $\Delta\delta^{15}\text{N}_{\text{hi-no}}$  values range from  $-3.67\text{‰}$  to  $5.34\text{‰}$ , with an average of  $0.51\text{‰}$ . The overall pattern of the  $\Delta\delta^{15}\text{N}_{\text{hi-no}}$  values shows that due to deposition, the atmospheric  $\text{NO}_x$  became isotopically lighter over the majority of the grids since EGU and vehicle  $\text{NO}_x$  is not being transported as far in the enhanced deposition. Conversely, in grids that contain or surround power plants and big cities the  $\delta^{15}\text{NO}_x$  increases because it is not as effectively mixing with low  $\delta^{15}\text{NO}_x$  from nearby grids. The enhanced deposition simulation somehow presents the isotope effects associated with the “pseudo photochemical transformation” of  $\text{NO}_x$  into  $\text{NO}_y$ . The complete isotope effect of tropospheric photochemistry will be addressed in future work, which incorporates  $^{15}\text{N}$  into the chemical mechanism of CMAQ for the simulation.

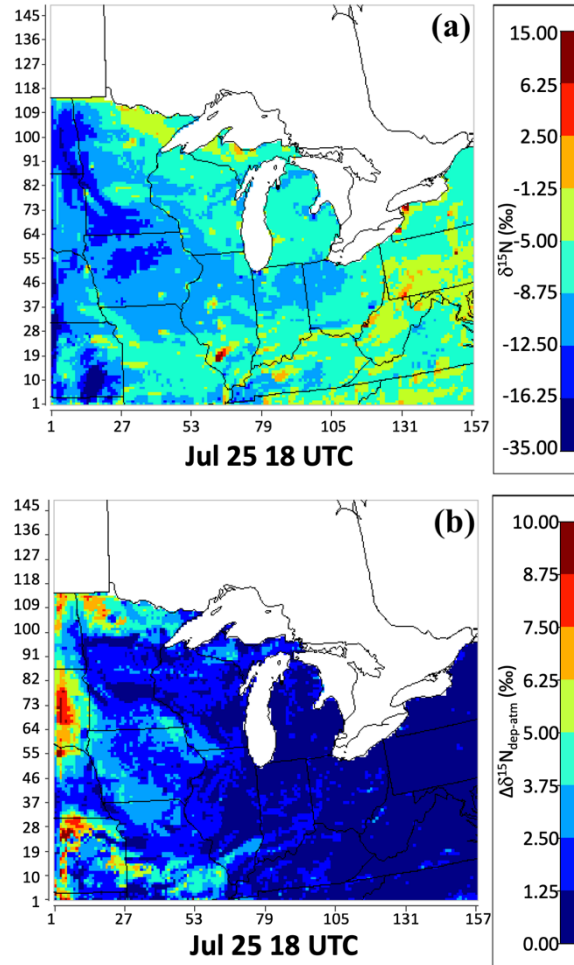


Figure 13: The  $\delta^{15}\text{N}$  values of  $\text{NO}_x$  deposition under the “enhanced deposition” scenario (a); the  $\Delta\delta^{15}\text{N}_{\text{dep-atm}}$  (b), at 18 UTC on July 25, are presented by color in each grid (NEI-2002 and 2016 meteorology). The warmer the color, the higher  $\delta^{15}\text{N}$  and  $\Delta\delta^{15}\text{N}_{\text{deposition}}$  values of atmospheric  $\text{NO}_x$

The  $\delta^{15}\text{NO}_x$  deposition (proxy for  $\delta^{15}\text{NO}_3^-$ ) simulated by CMAQ at these sites show similar monthly variations and seasonal trends as SMOKE (Fig. S19). The ranges of  $\delta^{15}\text{N}(\text{NO}_x)$  values within each month were narrower, comparing to the simulation from SMOKE, with a minimum during February (-8.7~ -4.4‰) and a maximum during August (-11.8~-4.2‰). The seasonal trend shows low  $\delta^{15}\text{N}(\text{NO}_x)$  during summer, with the median around -7.4‰, and high  $\delta^{15}\text{N}(\text{NO}_x)$  during winter, with the median around -6.0‰. Therefore, the CMAQ simulation inherits the monthly variations and seasonal trends from SMOKE, while the atmospheric  $\text{NO}_x$  becomes isotopically heavier, after taking atmospheric mixing and transport into account. As mentioned above, most of the NADP sites are located away from big cities and power plants. Thus, the atmospheric mixing and transport led to the isotopically heavier atmospheric  $\text{NO}_x$ .

1

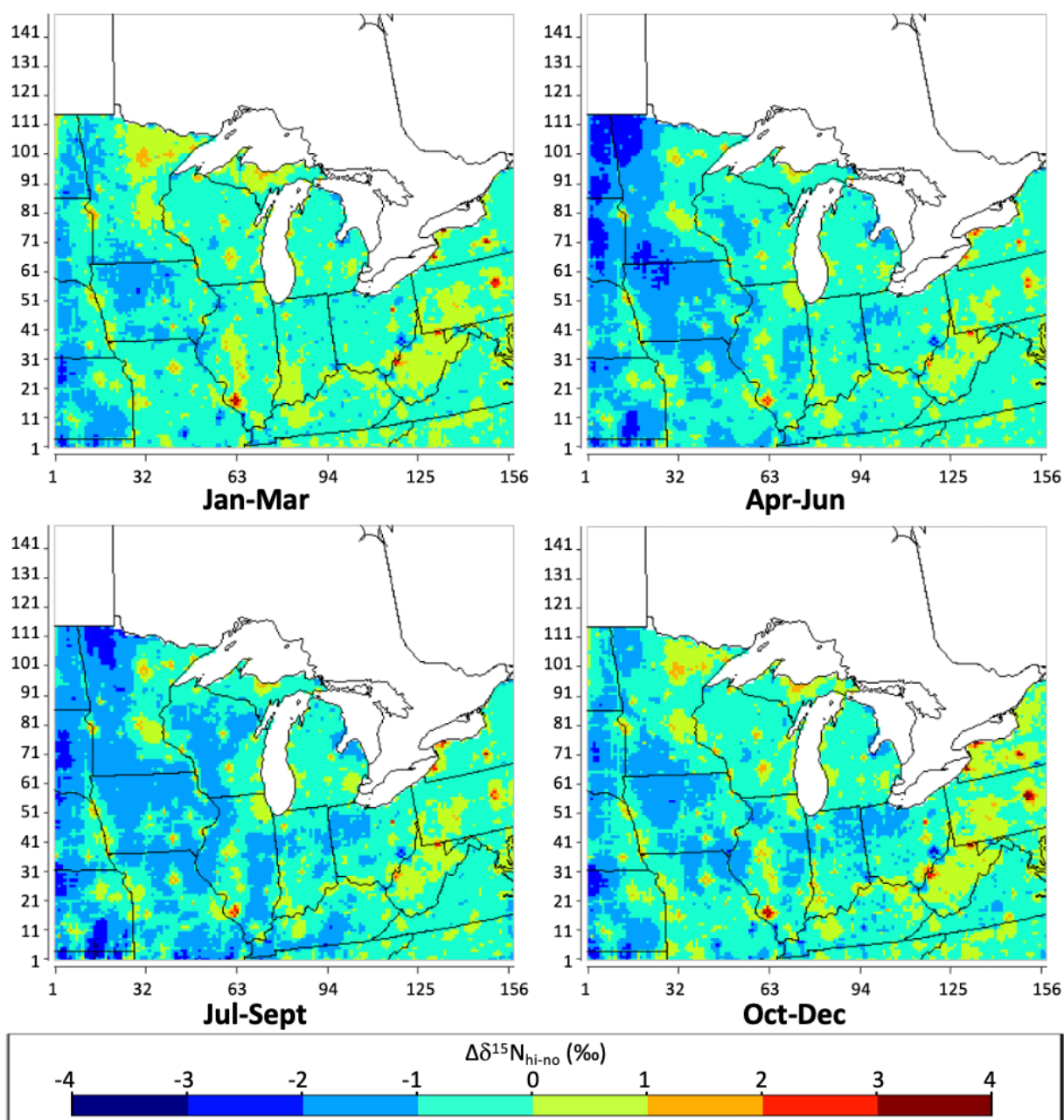


Figure 14: The difference between the  $\delta^{15}\text{N}$  (‰) value of atmospheric  $\text{NO}_x$  under the “enhanced deposition” scenario and “no deposition” scenario ( $\Delta\delta^{15}\text{N}_{\text{hi-no}}$ ) during each season (Winter: Jan-Mar; Spring: Apr-Jun; Summer: Jul-Sept; Fall: Oct-Dec), throughout the Midwest simulated by CMAQ, based on NEI-2002 and 2016 meteorology.

2

3 3.6 Model-observation comparison of  $\delta^{15}\text{NO}_x$

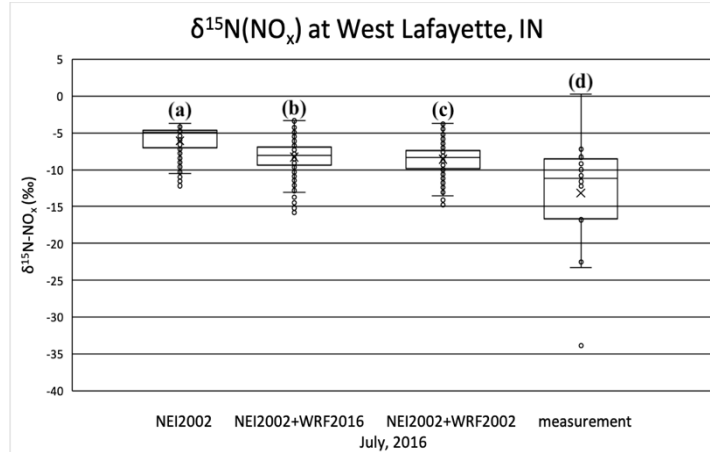


Figure 15: The  $\delta^{15}\text{NO}_x$  distributions for Lafayette, IN from July 8 to August 5, simulated by SMOKE (a), CMAQ based on 2016 (b) and 2002 meteorology (c), compare with the measured  $\delta^{15}\text{NO}_x$  (d) taken on July to August in 2016 (box: lower quartile, median, upper quartile; whisker: lower extreme, upper extreme; dots outside the whisker: outliers)

In order to evaluate the SMOKE/CMAQ simulations of atmospheric  $\delta^{15}\text{N}$ , they were compared to several existing observational datasets. The  $\delta^{15}\text{N}$  values under the “no transport” simulation by SMOKE in West Lafayette, IN was compared with the measurement (Walters, Fang, & Michalski, 2018) from July 8 to August 5, 2016 (Fig. 15). The range of SMOKE simulated  $\delta^{15}\text{N}(\text{NO}_x)$  from NEI-2002 ranges from -12.2‰ to -3.8‰, which is within the range of the corresponding measurement (-33.8 ~ 0.2 ‰). Whereas the median ( $-5.0 \pm 2.2$  ‰) of SMOKE simulated  $\delta^{15}\text{N}(\text{NO}_x)$  is higher than the median ( $-11.2 \pm 8.0$  ‰) of the measured values. The SMOKE simulated  $\delta^{15}\text{N}(\text{NO}_x)$  values in West Lafayette, IN are higher than the corresponding measurements. Therefore, the emission from the soil, livestock waste, off-road vehicles, and natural gas power plant might be underestimated, and/or the emission from the on-road vehicle and coal-fired power plant might be overestimated for both versions of NEI.

In addition to the effects from  $\text{NO}_x$  emission sources, the lower values and greater variations in measured  $\delta^{15}\text{N}(\text{NO}_x)$  might also be caused by the atmospheric mixing with the emission from surrounding grids, driven by the atmospheric processes. The  $\delta^{15}\text{N}$  of atmospheric  $\text{NO}_x$  under the “with transport” scenario by CMAQ with different meteorology conditions (simulated by WRF for the year 2002 and 2016) was compared with the measurement (Walters, Fang, & Michalski, 2018) from July 8 to August 5, 2016 (Fig. 15). The  $\delta^{15}\text{N}$  of atmospheric  $\text{NO}_x$  simulated based on 2016 meteorology ranges from -15.8‰ to -3.4‰, with the medium of  $-8.1 \pm 2.1$ ‰; the  $\delta^{15}\text{N}$  of atmospheric  $\text{NO}_x$  simulated based 2002 meteorology ranges from -14.8‰ to -3.7‰, with the medium of  $-8.4 \pm 1.9$ ‰. The  $\delta^{15}\text{N}$  of the corresponding measurement ranges from -33.8‰ to 0.2‰, with the medium of  $-11.2 \pm 8.0$ ‰. In general, the CMAQ simulations of  $\delta^{15}\text{N}(\text{NO}_x)$  under both of the scenarios conducted in this study perform better than the SMOKE simulation of  $\delta^{15}\text{N}(\text{NO}_x)$ , which only takes the variability of the  $\text{NO}_x$  emission source into account (Table S7).

### 3.7 Enhanced $\text{NO}_x$ deposition simulating $\delta^{15}\text{NO}_3$ : model observation comparison

1       The model was used to predict  $\delta^{15}\text{NO}_3^-$  and compared with the  $\delta^{15}\text{NO}_3^-$  in deposition collect  
2 between 2001 and 2003 at several Midwestern NADP sites (Table S4). The measurements of  $\delta^{15}\text{N}$   
3 values of  $\text{NO}_3^-$  at NADP sites from prior studies (Mase, 2010; Riha, 2013) show the similar  
4 monthly variations and seasonal trend as both “no transport” and “with transport” simulations (Fig.  
5 S19). There is a wide range of  $\delta^{15}\text{N}(\text{NO}_3^-)$  values within each month, with a minimum during  
6 January (10.4~17.2‰) and a maximum during August (1.0~16.7‰). The seasonal trend shows  
7 low  $\delta^{15}\text{N}(\text{NO}_3^-)$  during spring, with the median around 9.3‰, and high  $\delta^{15}\text{N}(\text{NO}_3^-)$  during winter,  
8 with the median around 13.0‰. The measured  $\delta^{15}\text{N}$  values of  $\text{NO}_3^-$  have the same seasonal trend  
9 as the simulated  $\delta^{15}\text{N}$  values of  $\text{NO}_x$ . Even considering the effect of atmospheric mixing and  
10 transport, the measured  $\delta^{15}\text{N}$  values of  $\text{NO}_3^-$  is about 17‰ higher than the simulated  $\delta^{15}\text{N}$  values  
11 of  $\text{NO}_x$ . The difference between CMAQ simulated and measured  $\delta^{15}\text{N}$  values of deposition is  
12 caused by the following two factors: a). the mixture of isotopically lighter  $\text{NO}_x$  from the  
13 surrounding area discussed in section 3.3, and b). the net N isotope effect during the conversion of  
14  $\text{NO}_x$  to  $\text{NO}_3^-$ , which will be addressed in future work.  
15

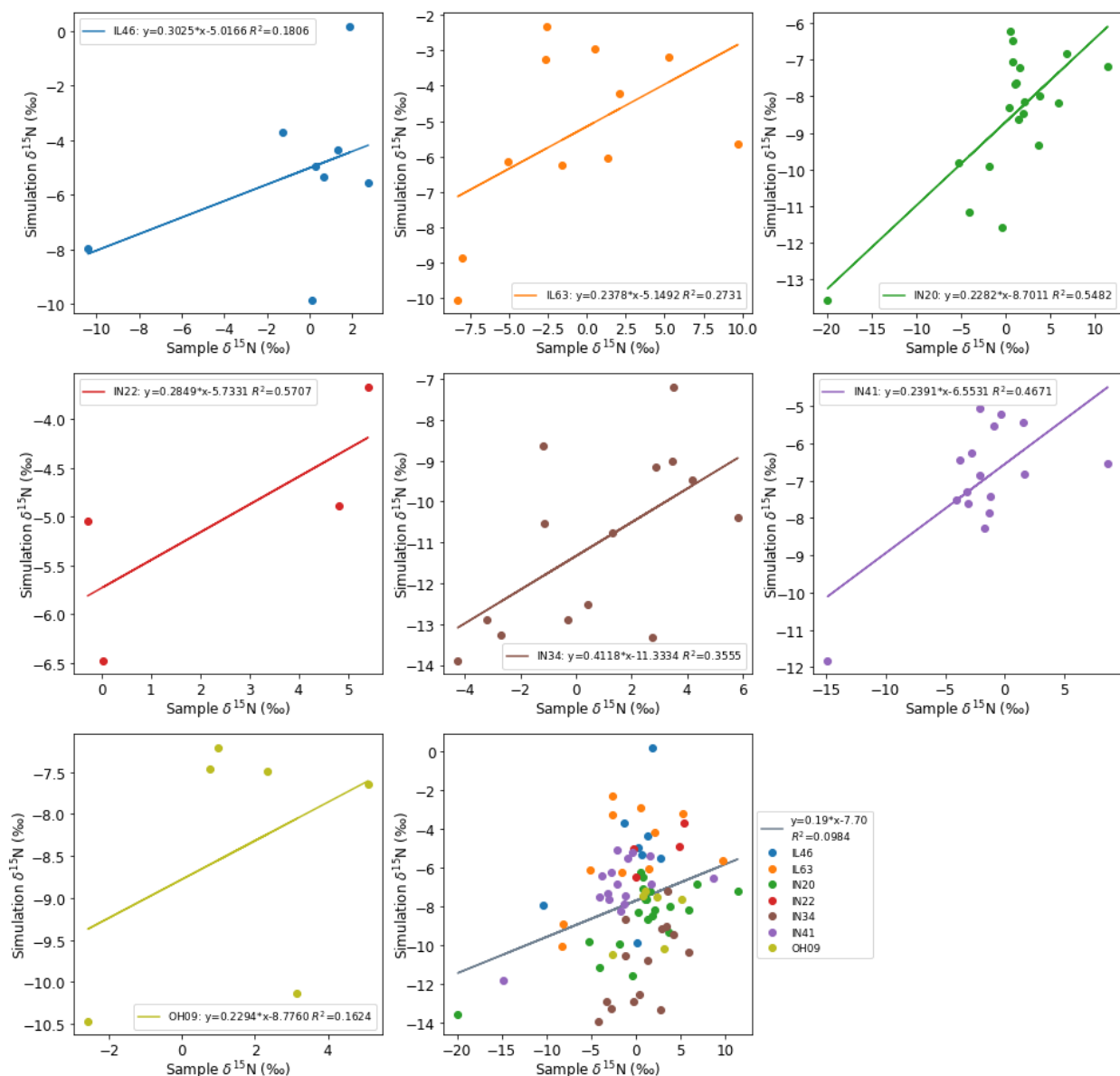


Figure 16: The emission + mixing + deposition CMAQ predicted  $\delta^{15}\text{N}$  value of  $\text{NO}_x$  deposition using NEI-2002 and 2002 meteorology compared to the measured  $\delta^{15}\text{N}$  of rain  $\text{NO}_3^-$  at NADP sites within IN, IL, and OH.

The 30 fold enhanced  $\text{NO}_x$  deposition (see methods) was used to simulate the  $\delta^{15}\text{N}$  value of  $\text{NO}_3^-$  deposition ( $\delta^{15}\text{N}(\text{NO}_3^-)$ ) that was then compared to observations (Fig. 16). As previously noted, rather than explicitly converting  $\text{NO}_x$  into  $\text{NO}_y$  via the chemical mechanism in CMAQ, which would require writing an isotope-enabled chemical scheme with appropriate rate constants, we amplified  $\text{NO}_x$  deposition as a surrogate. This amplification reduced the  $\text{NO}_x$  lifetime to about 1 day, thus by calculating the  $\delta^{15}\text{N}$  of  $\text{NO}_x$  in the deposition fraction, as opposed to residual  $\text{NO}_x$  in the atmosphere, we are approximating the  $\delta^{15}\text{N}(\text{NO}_3^-)$  in deposition. The model approximation was compared to  $\text{NO}_3^-$  collected at NADP sites within Indiana, Illinois, and Ohio in the year 2002 (Table S4). The NEI-2002 and WRF2002 were used for the SMOKE emission model and CMAQ simulations, respectively. The  $\delta^{15}\text{N}(\text{NO}_3^-)$  value in deposition was calculated by  $\delta^{15}\text{N}(\text{NO}_3^-) = \Sigma$

$f_{\text{NO}_x\text{hr}} \delta^{15}\text{N}(\text{NO}_x)_{\text{hr}}$ , where  $f_{\text{NO}_x\text{hr}}$  is the hourly mole fraction of  $\text{NO}_x$  isotopologue deposited ( $f_{\text{NO}_x\text{hr}} = \text{NO}_{x\text{hr}}/\text{NO}_{x\text{T}}$ ) and  $\delta^{15}\text{N}(\text{NO}_x)_{\text{hr}}$  is the  $\delta^{15}\text{N}$  value of  $\text{NO}_x$  in deposition. The total  $\text{NO}_x$  deposited ( $\text{NO}_{x\text{T}}$ ) used to calculate  $f_{\text{NO}_x\text{hr}}$  was the amount deposited 5 days prior to the sampling date since the NADP deposition collection integrate the week. The  $\delta^{15}\text{N}$  values of  $\text{NO}_x$  deposition simulated by CMAQ under the “enhanced deposition” scenario at each site were compared with the measurements of  $\delta^{15}\text{N}$  values of  $\text{NO}_3$  from prior studies (Mase, 2010; Riha, 2013). The scatter plots show moderate positive correlation between sample  $\delta^{15}\text{N}$  and simulated  $\delta^{15}\text{N}$ , with  $R^2$  between 0.16 and 0.57 (Fig. 16). The difference in the trend line equations among the NADP sites might be caused by the difference in air temperature and photolysis rate, which impact the chemical mechanisms converting  $\text{NO}_x$  into  $\text{NO}_y$  and will be explored in future study.

#### 4. Conclusion

The  $\delta^{15}\text{N}$  of atmospheric  $\text{NO}_x$  was simulated by SMOKE, by considering the  $\text{NO}_x$  emissions from NEI emission sectors and the corresponding  $\delta^{15}\text{N}$  values from previous research.  $\delta^{15}\text{N}$  is an effective tool to track the atmospheric  $\text{NO}_x$ , in terms of its evolution of spatial and temporal composition, altered by atmospheric processes. The simulation indicates that the  $\text{NO}_x$  emission from biogenic sources is the key driver for the variation of  $\delta^{15}\text{N}$ , especially among the NADP sites. The uncertainties in the  $\delta^{15}\text{N}(\text{NO}_x)$  simulation are less than 5% over the majority of the grids within the Midwest. For the  $\text{NO}_x$  emission from the regions dominated by biogenic source, the uncertainties in the  $\delta^{15}\text{N}(\text{NO}_x)$  simulation are less than 10%. The uncertainties in the  $\delta^{15}\text{N}(\text{NO}_x)$  simulation were well below the difference among the  $\delta^{15}\text{N}(\text{NO}_x)$  values from different  $\text{NO}_x$  emission sources (Fig. S20). Comparing with the measurements of  $\delta^{15}\text{N}(\text{NO}_3^-)$  from NADP sites within Indiana, Illinois, Ohio, and Kentucky, the simulated  $\delta^{15}\text{N}$  agreed well with the seasonal trend and monthly variation. While the simulated  $\text{NO}_x$  is slightly heavier than the corresponding measurements in West Lafayette, IN, taken from July to August 2016. According to the previous research, the uncertainty of  $\text{NO}_x$  emission is 71-250% from soil and 10-15% from the vehicle. The variations among the removal efficiency of different emission control technologies vary from 30% to 90%, also causes the uncertainty of power plant  $\text{NO}_x$  emission. In addition, in this study, due to the lack of measurements, the  $\delta^{15}\text{N}$  of coal-fired and natural gas non-EGUs (industrial boilers, commercial and residential fuel combustions) were assumed to be the same as the  $\delta^{15}\text{N}$  of coal-fired and natural gas EGUs respectively. Thus, detailed measurements of the  $\delta^{15}\text{N}$  of non-EGUs are necessary for future study. Besides this, the non-road vehicles (aircraft, ships, and trains) also need to be included in the future study.

If we only consider the effects from  $\text{NO}_x$  emission sources, the emission from soil, livestock waste, off-road vehicles, and natural gas power plant in West Lafayette, IN are possible to be underestimated, and the emission from the on-road vehicle and coal-fired power plant in West Lafayette, IN are possible to be overestimated. Another reason causing the estimated  $\text{NO}_x$  isotopically heavier than measured  $\text{NO}_x$  is the mixing caused by atmospheric processes, since the  $\text{NO}_x$  emission from the surrounding region of West Lafayette, IN is lighter. In addition, the tropospheric photochemistry could also alter the  $\delta^{15}\text{N}$  values during the processes that convert  $\text{NO}_x$  to  $\text{NO}_y$ .

After considering the impacts of atmospheric processes, by simulating CMAQ based on the  $^{15}\text{N}$  incorporated emission input datasets and the meteorology input dataset simulated from WRF and MCIP, the performance of the simulated  $\delta^{15}\text{N}(\text{NO}_x)$  is better. The simulation indicates that the PBL height is the key driver for the mixture of anthropogenic and natural  $\text{NO}_x$  emission, which deepens the gap between  $\delta^{15}\text{N}$  of atmospheric  $\text{NO}_x$  and  $\text{NO}_x$  emission. After considering the effects



1 of NO<sub>x</sub> emission sources and atmospheric processes, there is still an obvious gap between the  
2 simulated  $\delta^{15}\text{N}(\text{NO}_x)$  and the corresponding measurements. Therefore, before adjusting the NO<sub>x</sub>  
3 emission inventory, the future work is to explore how tropospheric photochemistry alters  
4  $\delta^{15}\text{N}(\text{NO}_x)$  by incorporating <sup>15</sup>N into the chemical mechanism of CMAQ and comparing the  
5 simulation with the corresponding measurements. With the validation of our nitrogen isotopes  
6 incorporated CMAQ, the NO<sub>x</sub> emission inventories could be effectively evaluated and improved.

7  
8 **Data availability:** The source code for SMOKE version 4.6 is available at  
9 [https://github.com/CEMPD/SMOKE/releases/tag/SMOKEv46\\_Sep2018](https://github.com/CEMPD/SMOKE/releases/tag/SMOKEv46_Sep2018). The source code for  
10 CMAQ version 5.2.1 is available at <https://github.com/USEPA/CMAQ/tree/5.2.1>. The in-detail  
11 simulation results for  $\delta^{15}\text{N}$  of NO<sub>x</sub> emission based on 2002 and 2016 versions of National Emission  
12 Inventory and the associated python codes are achieved on Zenodo.org (10.5281/zenodo.4048992).  
13 The input datasets for WRF simulation are available at <https://www.ncei.noaa.gov/data/>. The in-  
14 detail simulation results for  $\delta^{15}\text{N}$  of atmospheric NO<sub>x</sub> under all scenarios discussed in this paper  
15 and the CMAQ-based c-shell script for generating BCON for extracted domain simulation are  
16 achieved on Zenodo.org (10.5281/zenodo.4311986).

17  
18 **Author contributions:** Huan Fang and Greg Michalski were the investigator for the project and  
19 organized the tasks. Huan Fang develop the model codes, performed the simulation to incorporate  
20 <sup>15</sup>N into SMOKE outputs and generated  $\delta^{15}\text{N}$  values and reconstruct CMAQ by incorporating <sup>15</sup>N,  
21 and performed the simulation to generate  $\delta^{15}\text{N}$  values. Greg Michalski helped Huan Fang in  
22 interpreting the results. Huan Fang prepared the manuscript with contributions from all co-authors.

23  
24 **Acknowledgments:** We would like to thank the Purdue Research Foundation and the Purdue  
25 Climate Change Research Center for providing funding for the project. We would like to thank  
26 Scott Spak from School of Urban & Regional Planning, University of Iowa for simulating SMOKE  
27 using NEI-2002. We would like to thank Tomas Ratkus from Department of Earth, Atmospheric,  
28 and Planetary Sciences, Steven Plite, and Frank Bakhit from Rosen Center for Advanced  
29 Computing, Purdue University for setting up CMAQ on Purdue research computing for this project.



## References:

- Almaraz, M., Bai, E., Wang, C., Trousdell, J., Conley, S., Faloon, I. and Houlton, B. Z.: Agriculture is a major source of NO<sub>x</sub> pollution in California, *Sci. Adv.*, doi:10.1126/sciadv.aao3477, 2018.
- Ammann, M., Siegwolf, R., Pichlmayer, F., Suter, M., Saurer, M. and Brunold, C.: Estimating the uptake of traffic-derived NO<sub>2</sub> from <sup>15</sup>N abundance in Norway spruce needles, *Oecologia*, doi:10.1007/s004420050710, 1999.
- Beirle, S., Spichtinger, N., Stohl, A., Cummins, K. L., Turner, T., Boccippio, D., Cooper, O. R., Wenig, M., Grzegorski, M., Platt, U. and Wagner, T.: Estimating the NO<sub>x</sub> produced by lightning from GOME and NLDN data: A case study in the Gulf of Mexico, *Atmos. Chem. Phys.*, doi:10.5194/acp-6-1075-2006, 2006.
- Boersma, K. F., Eskes, H. J., Meijer, E. W. and Kelder, H. M.: Estimates of lightning NO<sub>x</sub> production from GOME satellite observations, *Atmos. Chem. Phys.*, doi:10.5194/acp-5-2311-2005, 2005.
- Bradshaw, J., Davis, D., Grodzinsky, G., Smyth, S., Newell, R., Sandholm, S. and Liu, S.: Observed distributions of nitrogen oxides in the remote free troposphere from the NASA Global Tropospheric Experiment programs, *Rev. Geophys.*, doi:10.1029/1999RG900015, 2000.
- Byun, D., Pleim, J., Tang, R. and Bourgeois, A.: Meteorology-Chemistry Interface Processor (MCIP) for Models-3 Community Multiscale Air Quality (CMAQ) Modeling System, System, 1999.
- Chameides, W. L., Davis, D. D., Bradshaw, J., Rodgers, M., Sandholm, S. and Bai, D. B.: An estimate of the NO<sub>x</sub> production rate in electrified clouds based on NO observations from the GTE/CITE 1 fall 1983 field operation, *J. Geophys. Res.*, doi:10.1029/jd092id02p02153, 1987.
- Chang, Y., Zhang, Y., Tian, C., Zhang, S., Ma, X., Cao, F., Liu, X., Zhang, W., Kuhn, T. and Lehmann, M. F.: Nitrogen isotope fractionation during gas-to-particle conversion of NO<sub>x</sub> to NO<sub>3</sub><sup>-</sup> in the atmosphere - Implications for isotope-based NO<sub>x</sub> source apportionment, *Atmos. Chem. Phys.*, doi:10.5194/acp-18-11647-2018, 2018.
- Christian, H. J., Blakeslee, R. J., Boccippio, D. J., Boeck, W. L., Buechler, D. E., Driscoll, K. T., Goodman, S. J., Hall, J. M., Koshak, W. J., Mach, D. M. and Stewart, M. F.: Global frequency and distribution of lightning as observed from space by the Optical Transient Detector, *J. Geophys. Res. Atmos.*, doi:10.1029/2002jd002347, 2003.
- Cicero-Fernández, P., Long, J. R. and Winer, A. M.: Effects of Grades and Other Loads on On-Road Emissions of Hydrocarbons and Carbon Monoxide, *J. Air Waste Manag. Assoc.*, doi:10.1080/10473289.1997.10464455, 1997.
- Dameris, M., Grewe, V., Ponater, M., Deckert, R., Eyring, V., Mager, F., Matthes, S., Schnadt, C., Stenke, A., Steil, B., Brühl, C. and Giorgetta, M. A.: Long-term changes and variability in a

transient simulation with a chemistry-climate model employing realistic forcing, *Atmos. Chem. Phys.*, doi:10.5194/acp-5-2121-2005, 2005.

Davidson, E. A.: Pulses of nitric oxide and nitrous oxide flux following wetting of dry soil: an assessment of probable sources and importance relative to annual fluxes, *Trace gas Exch. a Glob. Perspect.*, 1992.

Davidson, E. A. and Kingerlee, W.: A global inventory of nitric oxide emissions from soils, *Nutr. Cycl. Agroecosystems*, doi:10.1023/a:1009738715891, 1997.

de Foy, B., Lu, Z., Streets, D. G., Lamsal, L. N. and Duncan, B. N.: Estimates of power plant NO<sub>x</sub> emissions and lifetimes from OMI NO<sub>2</sub> satellite retrievals, *Atmos. Environ.*, doi:10.1016/j.atmosenv.2015.05.056, 2015.

De Laeter, J. R., Böhlke, J. K., De Bièvre, P., Hidaka, H., Peiser, H. S., Rosman, K. J. R. and Taylor, P. D. P.: Atomic weights of the elements: Review 2000 (IUPAC Technical Report), *Pure Appl. Chem.*, doi:10.1351/pac200375060683, 2003.

DeCaria, A. J., Pickering, K. E., Stenchikov, G. L. and Ott, L. E.: Lightning-generated NO<sub>x</sub> and its impact on tropospheric ozone production: A three-dimensional modeling study of a Stratosphere-Troposphere Experiment: Radiation, Aerosols and Ozone (STERAO-A) thunderstorm, *J. Geophys. Res. D Atmos.*, doi:10.1029/2004JD005556, 2005.

Dentener, F. J. and Crutzen, P. J.: Reaction of N<sub>2</sub>O<sub>5</sub> on tropospheric aerosols: impact on the global distributions of NO<sub>x</sub>, O<sub>3</sub>, and OH, *J. Geophys. Res.*, doi:10.1029/92JD02979, 1993.

Dignon, J. and Hameed, S.: Global emissions of nitrogen and sulfur oxides from 1860 to 1980, *J. Air Waste Manag. Assoc.*, doi:10.1080/08940630.1989.10466519, 1989.

Dreher, D. B. and Harley, R. A.: A fuel-based inventory for heavy-duty diesel truck emissions, *J. Air Waste Manag. Assoc.*, doi:10.1080/10473289.1998.10463686, 1998.

Duncan, B. N., Yoshida, Y., De Foy, B., Lamsal, L. N., Streets, D. G., Lu, Z., Pickering, K. E. and Krotkov, N. A.: The observed response of Ozone Monitoring Instrument (OMI) NO<sub>2</sub> columns to NO<sub>x</sub> emission controls on power plants in the United States: 2005-2011, *Atmos. Environ.*, doi:10.1016/j.atmosenv.2013.08.068, 2013.

Elliott, E. M., Kendall, C., Boyer, E. W., Burns, D. A., Lear, G. G., Golden, H. E., Harlin, K., Bytnerowicz, A., Butler, T. J. and Glatz, R.: Dual nitrate isotopes in dry deposition: Utility for partitioning NO<sub>x</sub> source contributions to landscape nitrogen deposition, *J. Geophys. Res. Biogeosciences*, doi:10.1029/2008JG000889, 2009.

Elliott, E. M., Kendall, C., Wankel, S. D., Burns, D. A., Boyer, E. W., Harlin, K., Bain, D. J. and Butler, T. J.: Nitrogen isotopes as indicators of NO<sub>x</sub> source contributions to atmospheric nitrate deposition across the midwestern and northeastern United States, *Environ. Sci. Technol.*, doi:10.1021/es070898t, 2007.

- 1
- 2 Farrell, A., Carter, R. and Rauber, R.: The NO<sub>x</sub> Budget: Market-based control of tropospheric
- 3 ozone in the northeastern United States, *Resour. Energy Econ.*, doi:10.1016/S0928-
- 4 7655(98)00035-9, 1999.
- 5
- 6 Fehr, T., Höller, H. and Huntreiser, H.: Model study on production and transport of lightning-
- 7 produced NO<sub>x</sub> in a EULINOX supercell storm, *J. Geophys. Res. D Atmos.*,
- 8 doi:10.1029/2003JD003935, 2004.
- 9
- 10 Felix, J. D., Elliott, E. M. and Shaw, S. L.: Nitrogen isotopic composition of coal-fired power
- 11 plant NO<sub>x</sub>: Influence of emission controls and implications for global emission inventories,
- 12 *Environ. Sci. Technol.*, doi:10.1021/es203355v, 2012.
- 13
- 14 Felix, J. D. and Elliott, E. M.: The agricultural history of human-nitrogen interactions as
- 15 recorded in ice core  $\delta^{15}\text{N}$ -NO<sub>3</sub><sup>-</sup>, *Geophys. Res. Lett.*, doi:10.1002/grl.50209, 2013.
- 16
- 17 Felix, J. D. and Elliott, E. M.: Isotopic composition of passively collected nitrogen dioxide
- 18 emissions: Vehicle, soil and livestock source signatures, *Atmos. Environ.*,
- 19 doi:10.1016/j.atmosenv.2014.04.005, 2014.
- 20
- 21 Felix, J. D., Elliott, E. M., Avery, G. B., Kieber, R. J., Mead, R. N., Willey, J. D. and Mullaugh,
- 22 K. M.: Isotopic composition of nitrate in sequential Hurricane Irene precipitation samples:
- 23 Implications for changing NO<sub>x</sub> sources, *Atmos. Environ.*, doi:10.1016/j.atmosenv.2015.01.075,
- 24 2015.
- 25
- 26 Fang, H., Walters, W. W., Mase, D., and Michalski, G.: i<sub>N</sub>RACM: incorporating <sup>15</sup>N into the
- 27 Regional Atmospheric Chemistry Mechanism (RACM) for assessing the role photochemistry
- 28 plays in controlling the isotopic composition of NO<sub>x</sub>, NO<sub>y</sub>, and atmospheric nitrate, *Geosci.*
- 29 *Model Dev.*, 14, 5001–5022, <https://doi.org/10.5194/gmd-14-5001-2021>, 2021.
- 30
- 31 Fibiger, D. L., Hastings, M. G., Lew, A. F. and Peltier, R. E.: Collection of NO and NO<sub>2</sub> for
- 32 isotopic analysis of NO<sub>x</sub> emissions, *Anal. Chem.*, doi:10.1021/ac502968e, 2014.
- 33
- 34 Fraser, A., Goutail, F., McLinden, C. A., Melo, S. M. L. and Strong, K.: Lightning-produced
- 35 NO<sub>2</sub> observed by two ground-based UV-visible spectrometers at Vanscoy, Saskatchewan in
- 36 August 2004, *Atmos. Chem. Phys.*, doi:10.5194/acp-7-1683-2007, 2007.
- 37
- 38 Fujita, E. M., Croes, B. E., Bennett, C. L., Lawson, D. R., Lurmann, F. W. and Main, H. H.:
- 39 Comparison of emission inventory and ambient concentration ratios of CO, NMOG, and NO<sub>x</sub> in
- 40 California's South Coast Air Basin, *J. Air Waste Manag. Assoc.*,
- 41 doi:10.1080/10473289.1992.10466989, 1992.
- 42
- 43 Fujita, E. M., Campbell, D. E., Zielinska, B. B., Sagebiel, J. C., Bowen, J. L., Goliff, W. S.,
- 44 Stockwell, W. R. and Lawson, D. R.: Diurnal and weekday variations in the source contributions
- 45 of ozone precursors in California's South Coast Air Basin, *J. Air Waste Manag. Assoc.*,
- 46 doi:10.1080/10473289.2003.10466226, 2003.

1  
2 Fujita, E. M., Stockwell, W. R., Campbell, D. E., Keislar, R. E. and Lawson, D. R.: Evolution of  
3 the magnitude and spatial extent of the weekend ozone effect in California's South Coast Air  
4 Basin, 1981–2000, *J. Air Waste Manag. Assoc.*, doi:10.1080/10473289.2003.10466225, 2003.  
5  
6 Galbally, I. E. and Roy, C. R.: Loss of fixed nitrogen from soils by nitric oxide exhalation [11],  
7 *Nature*, doi:10.1038/275734a0, 1978. Gallardo, L. and Rodhe, H.: Oxidized nitrogen in the  
8 remote Pacific: The role of electrical discharges over the oceans, *J. Atmos. Chem.*,  
9 doi:10.1023/A:1005738402496, 1997.  
10  
11 Gallardo, L. and Rodhe, H.: Oxidized nitrogen in the remote Pacific: The role of electrical  
12 discharges over the oceans, *J. Atmos. Chem.*, doi:10.1023/A:1005738402496, 1997.  
13  
14 Galloway, J. N. and Cowling, E. B.: Reactive nitrogen and the world: 200 Years of change, in  
15 *Ambio.*, 2002.  
16  
17 Galloway, J. N., Dentener, F. J., Capone, D. G., Boyer, E. W., Howarth, R. W., Seitzinger, S. P.,  
18 Asner, G. P., Cleveland, C. C., Green, P. A., Holland, E. A., Karl, D. M., Michaels, A. F., Porter,  
19 J. H., Townsend, A. R. and Vörösmarty, C. J.: Nitrogen cycles: Past, present, and future,  
20 *Biogeochemistry*, doi:10.1007/s10533-004-0370-0, 2004.  
21  
22 Ganzeveld, L. N., Lelieveld, J., Dentener, F. J., Krol, M. C., Bouwman, A. J. and Roelofs, G. J.:  
23 Global soil-biogenic NOX emissions and the role of canopy processes, *J. Geophys. Res. Atmos.*,  
24 doi:10.1029/2001JD001289, 2002.  
25  
26 Garten, C. T.: Nitrogen isotope composition of ammonium and nitrate in bulk precipitation and  
27 forest throughfall, *Int. J. Environ. Anal. Chem.*, doi:10.1080/03067319208027017, 1992.  
28  
29 Gauss, M., Myhre, G., Isaksen, I. S. A., Grewe, V., Pitari, G., Wild, O., Collins, W. J., Dentener,  
30 F. J., Ellingsen, K., Gohar, L. K., Hauglustaine, D. A., Iachetti, D., Lamarque, J. F., Mancini, E.,  
31 Mickley, L. J., Prather, M. J., Pyle, J. A., Sanderson, M. G., Shine, K. P., Stevenson, D. S., Sudo,  
32 K., Szopa, S. and Zeng, G.: Radiative forcing since preindustrial times due to ozone change in  
33 the troposphere and the lower stratosphere, *Atmos. Chem. Phys.*, doi:10.5194/acp-6-575-2006,  
34 2006.  
35  
36 Grell, G. A., Dudhia, J., & Stauffer, D. R.: A description of the fifth-generation Penn State/NCAR  
37 mesoscale model (MM5), NCAR Technical Note NCAR/TN-398+ STR, 1994.  
38  
39 Hall, S. J., Ogata, E. M., Weintraub, S. R., Baker, M. A., Ehleringer, J. R., Czimczik, C. I. and  
40 Bowling, D. R.: Convergence in nitrogen deposition and cryptic isotopic variation across urban  
41 and agricultural valleys in northern Utah, *J. Geophys. Res. Biogeosciences*,  
42 doi:10.1002/2016JG003354, 2016.  
43  
44 Hanson, P. J. and Lindberg, S. E.: Dry deposition of reactive nitrogen compounds: A review of  
45 leaf, canopy and non-foliar measurements, *Atmos. Environ. Part A, Gen. Top.*,  
46 doi:10.1016/0960-1686(91)90020-8, 1991.

- 1
- 2 Harley, R. A., McKeen, S. A., Pearson, J., Rodgers, M. O. and Lonneman, W. A.: Analysis of
- 3 motor vehicle emissions during the Nashville/Middle Tennessee Ozone Study, *J. Geophys. Res.*
- 4 *Atmos.*, doi:10.1029/2000JD900677, 2001.
- 5
- 6 Heaton, T. H. E.:  $^{15}\text{N}/^{14}\text{N}$  ratios of nitrate and ammonium in rain at Pretoria, South Africa,
- 7 *Atmos. Environ.*, doi:10.1016/0004-6981(87)90080-1, 1987.
- 8
- 9 Heaton, T. H. E.:  $^{15}\text{N}/^{14}\text{N}$  ratios of  $\text{NO}_x$  from vehicle engines and coal-fired power stations,
- 10 *Tellus B*, doi:10.1034/j.1600-0889.1990.00007.x-i1, 1990.
- 11
- 12 Hoering, T.: The isotopic composition of the ammonia and the nitrate ion in rain, *Geochim.*
- 13 *Cosmochim. Acta*, doi:10.1016/0016-7037(57)90021-2, 1957.
- 14
- 15 Houlton, B. Z., Boyer, E., Finzi, A., Galloway, J., Leach, A., Liptzin, D., Melillo, J., Rosenstock,
- 16 T. S., Sobota, D. and Townsend, A. R.: Intentional versus unintentional nitrogen use in the
- 17 United States: Trends, efficiency and implications, *Biogeochemistry*, doi:10.1007/s10533-012-
- 18 9801-5, 2013.
- 19
- 20 Houyoux, M.: Clean Air Interstate Rule Emissions Inventory Technical Support Document. US
- 21 EPA, 2005.
- 22
- 23 Hudman, R. C., Moore, N. E., Mebust, A. K., Martin, R. V., Russell, A. R., Valin, L. C. and
- 24 Cohen, R. C.: Steps towards a mechanistic model of global soil nitric oxide emissions:
- 25 Implementation and space based-constraints, *Atmos. Chem. Phys.*, doi:10.5194/acp-12-7779-
- 26 2012, 2012.
- 27
- 28 Huntrieser, H., Schlager, H., Feigl, C. and Höller, H.: Transport and production of  $\text{NO}_x$  in
- 29 electrified thunderstorms: Survey of previous studies and new observations at midlatitudes, *J.*
- 30 *Geophys. Res. Atmos.*, doi:10.1029/98JD02353, 1998.
- 31
- 32 Huntrieser, H., Feigl, C., Schlager, H., Schröder, F., Gerbig, C., van Velthoven, P., Flatøy, F.,
- 33 Théry, C., Petzold, A., Höller, H. and Schumann, U.: Airborne measurements of  $\text{NO}_x$ , tracer
- 34 species, and small particles during the European lightning nitrogen oxides experiment, *J.*
- 35 *Geophys. Res. Atmos.*, doi:10.1029/2000jd000209, 2002.
- 36
- 37 Ingalls, M. N.: On-road vehicle emission factors from measurements in a Los Angeles area
- 38 tunnel, in *Proceedings - A&WMA Annual Meeting.*, 1989.
- 39
- 40 Jacob, D. J. and Wofsy, S. C.: Budgets of reactive nitrogen, hydrocarbons, and ozone over the
- 41 Amazon forest during the wet season, *J. Geophys. Res.*, doi:10.1029/jd095id10p16737, 1990.
- 42
- 43 Jaeglé, L., Steinberger, L., Martin, R. V. and Chance, K.: Global partitioning of  $\text{NO}_x$  sources
- 44 using satellite observations: Relative roles of fossil fuel combustion, biomass burning and soil
- 45 emissions, in *Faraday Discussions.*, 2005.
- 46

- 1 Johansson, C.: Pine forest: a negligible sink for atmospheric NO<sub>x</sub> in rural Sweden , *Tellus B*  
2 *Chem. Phys. Meteorol.*, doi:10.3402/tellusb.v39i5.15360, 1987.
- 3
- 4 Kim, S. W., Heckel, A., Frost, G. J., Richter, A., Gleason, J., Burrows, J. P., McKeen, S., Hsie,  
5 E. Y., Granier, C. and Trainer, M.: NO<sub>2</sub> columns in the western United States observed from  
6 space and simulated by a regional chemistry model and their implications for NO<sub>x</sub> emissions, *J.*  
7 *Geophys. Res. Atmos.*, doi:10.1029/2008JD011343, 2009.
- 8
- 9 Koike, M., Kondo, Y., Kita, K., Takegawa, N., Nishi, N., Kashiara, T., Kawakami, S., Kudoh,  
10 S., Blake, D., Shirai, T., Liley, B., Ko, M. K., Miyazaki, Y., Kawasaki, Z. and Ogawa, T.:  
11 Measurements of reactive nitrogen produced by tropical thunderstorms during BIBLE-C, *J.*  
12 *Geophys. Res. Atmos.*, doi:10.1029/2006JD008193, 2007.
- 13
- 14 Laughner, J. L., & Cohen, R. C. (2019). Direct observation of changing NO<sub>x</sub> lifetime in North  
15 American cities. *Science*, 366(6466), 723-727.
- 16
- 17 Lawrence, M. G., Chameides, W. L., Kasibhatla, P. S., Levy, H. and Moxim, W.: Lightning and  
18 atmospheric chemistry: The rate of atmospheric NO production, in *Handbook of Atmospheric*  
19 *Electrodynamics.*, 2017.
- 20
- 21 Lerda, M. T., Munger, J. W. and Jacob, D. J.: The NO<sub>2</sub> flux conundrum, *Science* (80-. ),  
22 doi:10.1126/science.289.5488.2291, 2000.
- 23
- 24 Levy, H., Moxim, W. J. and Kasibhatla, P. S.: A global three-dimensional time-dependent  
25 lightning source of tropospheric NO<sub>x</sub>, *J. Geophys. Res. Atmos.*, doi:10.1029/96jd02341, 1996.
- 26
- 27 Li, D. and Wang, X.: Nitrogen isotopic signature of soil-released nitric oxide (NO) after fertilizer  
28 application, *Atmos. Environ.*, doi:10.1016/j.atmosenv.2008.01.042, 2008.
- 29
- 30 Li, Y., Schichtel, B. A., Walker, J. T., Schwede, D. B., Chen, X., Lehmann, C. M. B., Puchalski,  
31 M. A., Gay, D. A. and Collett, J. L.: Increasing importance of deposition of reduced nitrogen in  
32 the United States, *Proc. Natl. Acad. Sci. U. S. A.*, doi:10.1073/pnas.1525736113, 2016.
- 33
- 34 Liao, T., Gui, K., Jiang, W., Wang, S., Wang, B., Zeng, Z., Che, H., Wang, Y. and Sun, Y.: Air  
35 stagnation and its impact on air quality during winter in Sichuan and Chongqing, southwestern  
36 China, *Sci. Total Environ.*, doi:10.1016/j.scitotenv.2018.04.122, 2018.
- 37
- 38 Lighty, J. A. S., Veranth, J. M. and Sarofim, A. F.: Combustion aerosols: Factors governing their  
39 size and composition and implications to human health, *J. Air Waste Manag. Assoc.*,  
40 doi:10.1080/10473289.2000.10464197, 2000.
- 41
- 42 Liu, L., Guo, J., Miao, Y., Liu, L., Li, J., Chen, D., He, J. and Cui, C.: Elucidating the  
43 relationship between aerosol concentration and summertime boundary layer structure in central  
44 China, *Environ. Pollut.*, doi:10.1016/j.envpol.2018.06.008, 2018.
- 45

- 1 Lu, Z., Streets, D. G., De Foy, B., Lamsal, L. N., Duncan, B. N. and Xing, J.: Emissions of  
2 nitrogen oxides from US urban areas: Estimation from Ozone Monitoring Instrument retrievals  
3 for 2005-2014, *Atmos. Chem. Phys.*, doi:10.5194/acp-15-10367-2015, 2015.
- 4
- 5 Ludwig, J., Meixner, F. X., Vogel, B. and Forstner, J.: Soil-air exchange of nitric oxide: An  
6 overview of processes, environmental factors, and modeling studies, *Biogeochemistry*,  
7 doi:10.1023/A:1006424330555, 2001.
- 8
- 9 Martin, R. V., Sauvage, B., Folkins, I., Sioris, C. E., Booone, C., Bernath, P. and Ziemke, J.:  
10 Space-based constraints on the production of nitric oxide by lightning, *J. Geophys. Res. Atmos.*,  
11 doi:10.1029/2006JD007831, 2007.
- 12
- 13 Mase, D. F.: A coupled modeling and observational approach to understanding oxygen-18 in  
14 atmospheric nitrate, Ph. D. thesis, Purdue University, United States of America, 2010.
- 15
- 16 McDonald, B. C., McKeen, S. A., Cui, Y. Y., Ahmadov, R., Kim, S. W., Frost, G. J., ... &  
17 Trainer, M.: Modeling ozone in the eastern US using a fuel-based mobile source emissions  
18 inventory, *Environmental science & technology*, 52(13), 7360-7370, 2018.
- 19
- 20 Miao, Y., Guo, J., Liu, S., Zhao, C., Li, X., Zhang, G., Wei, W. and Ma, Y.: Impacts of synoptic  
21 condition and planetary boundary layer structure on the trans-boundary aerosol transport from  
22 Beijing-Tianjin-Hebei region to northeast China, *Atmos. Environ.*,  
23 doi:10.1016/j.atmosenv.2018.03.005, 2018.
- 24
- 25 Miao, Y., Li, J., Miao, S., Che, H., Wang, Y., Zhang, X., Zhu, R. and Liu, S.: Interaction  
26 Between Planetary Boundary Layer and PM<sub>2.5</sub> Pollution in Megacities in China: a Review,  
27 *Curr. Pollut. Reports*, doi:10.1007/s40726-019-00124-5, 2019.
- 28
- 29 Miller, D. J., Wojtal, P. K., Clark, S. C. and Hastings, M. G.: Vehicle NO<sub>x</sub> emission plume  
30 isotopic signatures: Spatial variability across the eastern United States, *J. Geophys. Res.*,  
31 doi:10.1002/2016JD025877, 2017.
- 32
- 33 Miller, D. J., Chai, J., Guo, F., Dell, C. J., Karsten, H. and Hastings, M. G.: Isotopic Composition  
34 of In Situ Soil NO<sub>x</sub> Emissions in Manure-Fertilized Cropland, *Geophys. Res. Lett.*,  
35 doi:10.1029/2018GL079619, 2018.
- 36
- 37 Moore, H.: The isotopic composition of ammonia, nitrogen dioxide and nitrate in the  
38 atmosphere, *Atmos. Environ.*, doi:10.1016/0004-6981(77)90102-0, 1977.
- 39
- 40 Muller, J. F.: Geographical distribution and seasonal variation of surface emissions and  
41 deposition velocities of atmospheric trace gases, *J. Geophys. Res.*, doi:10.1029/91JD02757,  
42 1992.
- 43
- 44 Müller, J.-F. and Stavrakou, T.: Inversion of CO and NO<sub>x</sub> emissions using the adjoint of the  
45 IMAGES model, *Atmos. Chem. Phys.*, doi:10.5194/acp-5-1157-2005, 2005.
- 46

1 Murray, L. T.: Lightning NO<sub>x</sub> and Impacts on Air Quality, Curr. Pollut. Reports,  
2 doi:10.1007/s40726-016-0031-7, 2016.  
3  
4 National Centers for Environmental Information: U.S. Wind Climatology, Available from:  
5 <https://www.ncdc.noaa.gov/societal-impacts/wind/>, 2019.  
6  
7 National Centers for Environmental Information: Model Datasets, available from:  
8 <https://www.ncdc.noaa.gov/data-access/model-data/model-datasets>, 2019.  
9  
10 Occhipinti, C., Aneja, V. P., Showers, W. and Niyogi, D.: Back-trajectory analysis and source-  
11 receptor relationships: Particulate matter and nitrogen isotopic composition in rainwater,  
12 Journal of the Air and Waste Management Association., 2008.  
13  
14 Oke, T. R.: Boundary Layer Climates., 2002.  
15  
16 Ott, L. E., Pickering, K. E., Stenchikov, G. L., Huntrieser, H. and Schumann, U.: Effects of  
17 lightning NO<sub>x</sub> production during the 21 July European Lightning Nitrogen Oxides Project storm  
18 studied with a three-dimensional cloud-scale chemical transport model, J. Geophys. Res. Atmos.,  
19 doi:10.1029/2006JD007365, 2007.  
20  
21 Parrish, D. D.: Critical evaluation of US on-road vehicle emission inventories, Atmos. Environ.,  
22 doi:10.1016/j.atmosenv.2005.11.033, 2006.  
23  
24 Pearson, J., Wells, D. M., Seller, K. J., Bennett, A., Soares, A., Woodall, J. and Ingrouille, M. J.:  
25 Traffic exposure increases natural <sup>15</sup>N and heavy metal concentrations in mosses, New Phytol.,  
26 doi:10.1046/j.1469-8137.2000.00702.x, 2000.  
27  
28 Pierce, T. E.: Reconsideration of the Emission Factors assumed in BEIS3 for Three USGS  
29 Vegetation Categories: Shrubland, Coniferous Forest, and Deciduous Forest, 2001.  
30  
31 Pierson, W. R., Gertler, A. W. and Bradow, R. L.: Comparison of the scaqs tunnel study with  
32 other onroad vehicle emission data, J. Air Waste Manag. Assoc.,  
33 doi:10.1080/10473289.1990.10466799, 1990.  
34  
35 Pierson, W. R., Gertler, A. W., Robinson, N. F., Sagebiel, J. C., Zielinska, B., Bishop, G. A.,  
36 Stedman, D. H., Zweidinger, R. B. and Ray, W. D.: Real-world automotive emissions - summary  
37 of studies in the Fort McHenry and Tuscarora Mountain Tunnels, in Atmospheric Environment.,  
38 1996.  
39  
40 Pilegaard, K.: Processes regulating nitric oxide emissions from soils, Philos. Trans. R. Soc. B  
41 Biol. Sci., doi:10.1098/rstb.2013.0126, 2013.  
42  
43 Potter, C. S., Matson, P. A., Vitousek, P. M. and Davidson, E. A.: Process modeling of controls  
44 on nitrogen trace gas emissions from soils worldwide, J. Geophys. Res. Atmos.,  
45 doi:10.1029/95JD02028, 1996.  
46



- 1 Pouliot, G., & Pierce, T. E.: Integration of the Model of Emissions of Gases and Aerosols from  
2 Nature (MEGAN) into the CMAQ Modeling System, in: 18th International Emission Inventory  
3 Conference, Baltimore, Maryland, 14 April 2009, 14-17, 2009.
- 4
- 5 Redling, K., Elliott, E., Bain, D. and Sherwell, J.: Highway contributions to reactive nitrogen  
6 deposition: Tracing the fate of vehicular NO<sub>x</sub> using stable isotopes and plant biomonitors,  
7 Biogeochemistry, doi:10.1007/s10533-013-9857-x, 2013.
- 8
- 9 Ridley, B. A., Dye, J. E., Walega, J. G., Zheng, J., Grahek, F. E. and Rison, W.: On the  
10 production of active nitrogen by thunderstorms over New Mexico, J. Geophys. Res. Atmos.,  
11 doi:10.1029/96jd01706, 1996.
- 12
- 13 Ridley, B., Ott, L., Pickering, K., Emmons, L., Montzka, D., Weinheimer, A., Knapp, D.,  
14 Grahek, F., Li, L., Heymsfield, G., McGill, M., Kucera, P., Mahoney, M. J., Baumgardner, D.,  
15 Schultz, M. and Brasseur, G.: Florida thunderstorms: A faucet of reactive nitrogen to the upper  
16 troposphere, J. Geophys. Res. D Atmos., doi:10.1029/2004JD004769, 2004.
- 17
- 18 Riha, K. M.: The use of stable isotopes to constrain the nitrogen cycle, Ph. D. thesis, Purdue  
19 University, United States of America, 2013.
- 20
- 21 Russell, K. M., Galloway, J. N., MacKo, S. A., Moody, J. L. and Scudlark, J. R.: Sources of  
22 nitrogen in wet deposition to the Chesapeake Bay region, Atmos. Environ., doi:10.1016/S1352-  
23 2310(98)00044-2, 1998.
- 24
- 25 Savard, M. M., Bégin, C., Smirnoff, A., Marion, J. and Rioux-Paquette, E.: Tree-ring nitrogen  
26 isotopes reflect anthropogenic NO<sub>x</sub> emissions and climatic effects, Environ. Sci. Technol.,  
27 doi:10.1021/es802437k, 2009.
- 28
- 29 Savard, M. M., Cole, A., Smirnoff, A. and Vet, R.:  $\Delta^{15}\text{N}$  values of atmospheric N species  
30 simultaneously collected using sector-based samplers distant from sources – Isotopic inheritance  
31 and fractionation, Atmos. Environ., doi:10.1016/j.atmosenv.2017.05.010, 2017.
- 32
- 33 Sawyer, R. F., Harley, R. A., Cadle, S. H., Norbeck, J. M., Slott, R. and Bravo, H. A.: Mobile  
34 sources critical review: 1998 NARSTO assessment, Atmos. Environ., doi:10.1016/S1352-  
35 2310(99)00463-X, 2000.
- 36
- 37 Scholes, M. C., Martin, R., Scholes, R. J., Parsons, D. and Winstead, E.: NO and N<sub>2</sub>O emissions  
38 from savanna soils following the first simulated rains of the season, Nutr. Cycl. Agroecosystems,  
39 doi:10.1023/a:1009781420199, 1997.
- 40
- 41 Schumann, U., Kurz, C., Schlager, H., Huntrieser, H., Emmons, L., Labrador, L., Meijer, E.,  
42 Ulanovsky, A. and Viciani, S.: Towards a robust estimate of the global lightning nitrogen oxides  
43 source rate and its error bound, in European Space Agency, (Special Publication) ESA SP., 2006.
- 44
- 45 Schumann, U. and Huntrieser, H.: The global lightning-induced nitrogen oxides source, Atmos.  
46 Chem. Phys., doi:10.5194/acp-7-3823-2007, 2007.

1  
2 Schwartz, S. E.: The Whitehouse effect - Shortwave radiative forcing of climate by  
3 anthropogenic aerosols: An overview, *J. Aerosol Sci.*, doi:10.1016/0021-8502(95)00533-1, 1996.  
4  
5 Schwede, D., Pouliot, G. and Pierce, T.: Changes to the biogenic emissions inventory system  
6 version 3 (BEIS3), in 4th Annual CMAS User's Conference., 2005.  
7  
8 Selden, T. M., Forrest, A. S., & Lockhart, J. E.: Analyzing the reductions in US air pollution  
9 emissions: 1970 to 1990, *Land Economics*, 1-21, doi: 10.2307/3146990, 1999.  
10  
11 Shepherd, M. F., Barzetti, S. and Hastie, D. R.: The production of atmospheric NO<sub>x</sub> and N<sub>2</sub>O from  
12 a fertilized agricultural soil, *Atmos. Environ. Part A, Gen. Top.*, doi:10.1016/0960-  
13 1686(91)90277-E, 1991.  
14  
15 Shu, L., Xie, M., Gao, D., Wang, T., Fang, D., Liu, Q., Huang, A. and Peng, L.: Regional severe  
16 particle pollution and its association with synoptic weather patterns in the Yangtze River Delta  
17 region, China, *Atmos. Chem. Phys.*, doi:10.5194/acp-17-12871-2017, 2017.  
18  
19 Singer, B. C. and Harley, R. A.: A Fuel-Based Motor Vehicle Emission Inventory, *J. Air Waste*  
20 *Manag. Assoc.*, doi:10.1080/10473289.1996.10467492, 1996.  
21  
22 Singer, B. C. and Harley, R. A.: A fuel-based inventory of motor vehicle exhaust emissions in the  
23 Los Angeles area during summer 1997, *Atmos. Environ.*, doi:10.1016/S1352-2310(99)00358-1,  
24 2000.  
25  
26 Skamarock, W. C., Dye, J. E., Defer, E., Barth, M. C., Stith, J. L., Ridley, B. A. and Baumann, K.:  
27 Observational- and modeling-based budget of lightning-produced NO<sub>x</sub> in a continental  
28 thunderstorm, *J. Geophys. Res. Atmos.*, doi:10.1029/2002jd002163, 2003.  
29  
30 Slovik, S., Siegmund, A., Fuhrer, H. W. and Heber, U.: Stomatal uptake of SO<sub>2</sub>, NO<sub>x</sub> and O<sub>3</sub> by  
31 spruce crowns (*Picea abies*) and canopy damage in Central Europe, *New Phytol.*,  
32 doi:10.1111/j.1469-8137.1996.tb01884.x, 1996.  
33  
34 Snape, C. E., Sun, C., Fallick, A. E., Irons, R. and Haskell, J.: Potential of stable nitrogen isotope  
35 ratio measurements to resolve fuel and thermal NO<sub>x</sub> in coal combustion, *Fuel Chem. Div. Prepr.*,  
36 2003.  
37  
38 Snyder, J. P.: Map projections - a working manual, *US Geol. Surv. Prof. Pap.*, 1987.  
39  
40 Spak, S., Holloway, T., Mednick, A., & Stone, B.: Evaluation of Bottom-Up Mobile Emissions  
41 Inventories in the Upper Midwest, in: American Geophysical Union Fall Meeting, San Francisco,  
42 California, 10-14 Dec 2007, 2007.  
43  
44 Srivastava, R. K., Neuffer, W., Grano, D., Khan, S., Staudt, J. E. and Jozewicz, W.: Controlling  
45 NO<sub>x</sub> emission from industrial sources, *Environ. Prog.*, doi:10.1002/ep.10063, 2005.  
46

1 Staudt, A. C., Jacob, D. J., Ravetta, F., Logan, J. A., Bachiochi, D., Sandholm, S., Ridley, B.,  
2 Singh, H. B. and Talbot, B.: Sources and chemistry of nitrogen oxides over the tropical Pacific,  
3 J. Geophys. Res. Atmos., doi:10.1029/2002jd002139, 2003.

4

5 Stavrakou, T., Müller, J. F., Boersma, K. F., Van Der A., R. J., Kurokawa, J., Ohara, T. and  
6 Zhang, Q.: Key chemical NO<sub>x</sub> sink uncertainties and how they influence top-down emissions of  
7 nitrogen oxides, Atmos. Chem. Phys., doi:10.5194/acp-13-9057-2013, 2013.

8

9 Stehfest, E. and Bouwman, L.: N<sub>2</sub>O and NO emission from agricultural fields and soils under  
10 natural vegetation: Summarizing available measurement data and modeling of global annual  
11 emissions, Nutr. Cycl. Agroecosystems, doi:10.1007/s10705-006-9000-7, 2006.

12

13 Stevenson, D. S., Dentener, F. J., Schultz, M. G., Ellingsen, K., van Noije, T. P. C., Wild, O.,  
14 Zeng, G., Amann, M., Atherton, C. S., Bell, N., Bergmann, D. J., Bey, I., Butler, T., Cofala, J.,  
15 Collins, W. J., Derwent, R. G., Doherty, R. M., Drevet, J., Eskes, H. J., Fiore, A. M., Gauss, M.,  
16 Hauglustaine, D. A., Horowitz, L. W., Isaksen, I. S. A., Krol, M. C., Lamarque, J. F., Lawrence,  
17 M. G., Montanaro, V., Müller, J. F., Pitari, G., Prather, M. J., Pyle, J. A., Rast, S., Rodriguez, J.  
18 M., Sanderson, M. G., Savage, N. H., Shindell, D. T., Strahan, S. E., Sudo, K. and Szopa, S.:  
19 Multimodel ensemble simulations of present-day and near-future tropospheric ozone, J.  
20 Geophys. Res. Atmos., doi:10.1029/2005JD006338, 2006.

21

22 The Institute for the Environment - The University of North Carolina at Chapel Hill: SMOKE v4.5  
23 User's Manual, Available from: <https://www.cmascenter.org/smoke/documentation/4.5/html/>,  
24 2017.

25

26 Thoene, B., Rennenberg, H. and Weber, P.: Absorption of atmospheric NO<sub>2</sub> by spruce (*Picea*  
27 *abies*) trees: II. Parameterization of NO<sub>2</sub> fluxes by controlled dynamic chamber experiments,  
28 New Phytol., doi:10.1111/j.1469-8137.1996.tb04630.x, 1996.

29

30 Thomas, R. J., Krehbiel, P. R., Rison, W., Hamlin, T., Boccippio, D. J., Goodman, S. J. and  
31 Christian, H. J.: Comparison of ground-based 3-dimensional lightning mapping observations  
32 with satellite-based LIS observations in Oklahoma, Geophys. Res. Lett.,  
33 doi:10.1029/1999GL010845, 2000.

34

35 Tie, X., Zhang, R., Brasseur, G. and Lei, W.: Global NO<sub>x</sub> production by lightning, J. Atmos.  
36 Chem., doi:10.1023/A:1016145719608, 2002.

37

38 Tost, H., Jöckel, P. and Lelieveld, J.: Lightning and convection parameterisations - Uncertainties  
39 in global modelling, Atmos. Chem. Phys., doi:10.5194/acp-7-4553-2007, 2007.

40

41 United States Census Bureau: 2007–2011 American Community Survey 5-Year Estimates, travel  
42 time to work by zip code, table B08303, Available from: [https://www.census.gov/programs-](https://www.census.gov/programs-surveys/acs/technical-documentation/table-and-geography-changes/2011/5-year.html)  
43 [surveys/acs/technical-documentation/table-and-geography-changes/2011/5-year.html](https://www.census.gov/programs-surveys/acs/technical-documentation/table-and-geography-changes/2011/5-year.html), 2019.

44

45 United States Energy Information Administration: Electricity, Available from:  
46 <https://www.eia.gov/electricity/data/eia860/>, 2017a.

1  
2 United States Energy Information Administration: U.S. electric generating capacity increase in  
3 2016 was largest net change since 2011, Available from:  
4 <https://www.eia.gov/todayinenergy/detail.php?id=30112>, 2017b.  
5  
6 United States Environmental Protection Agency: National Emissions Inventory (NEI), Available  
7 from: <https://www.epa.gov/air-emissions-inventories/national-emissions-inventory-nei>, 2014.  
8  
9 United States Environmental Protection Agency: Biogenic Emissions Landuse Database,  
10 Available from: [https://www.epa.gov/air-emissions-modeling/biogenic-emissions-landuse-](https://www.epa.gov/air-emissions-modeling/biogenic-emissions-landuse-database-version-3-beld3)  
11 [database-version-3-beld3](https://www.epa.gov/air-emissions-modeling/biogenic-emissions-landuse-database-version-3-beld3), 2018a.  
12  
13 United States Environmental Protection Agency: 2002 National Emissions Inventory (NEI)  
14 Booklet, Available from: [https://archive.epa.gov/epa/air-emissions-inventories/2002-national-](https://archive.epa.gov/epa/air-emissions-inventories/2002-national-emissions-inventory-nei-booklet.html)  
15 [emissions-inventory-nei-booklet.html](https://archive.epa.gov/epa/air-emissions-inventories/2002-national-emissions-inventory-nei-booklet.html), 2018b  
16  
17 US Environmental Protection Agency: User's Guide to MOBILE6.1 and MOBILE6.2 Mobile  
18 Source Emission Factor Model, Tech. Rep. EPA420-R-03-010, 2003.  
19  
20 Van Noije, T. P. C., Eskes, H. J., Dentener, F. J., Stevenson, D. S., Ellingsen, K., Schultz, M. G.,  
21 Wild, O., Amann, M., Atherton, C. S., Bergmann, D. J., Bey, I., Boersma, K. F., Butler, T.,  
22 Cofala, J., Drevet, J., Fiore, A. M., Gauss, M., Hauglustaine, D. A., Horowitz, L. W., Isaksen, I.  
23 S. A., Krol, M. C., Lamarque, J. F., Lawrence, M. G., Martin, R. V., Montanaro, V., Müller, J.  
24 F., Pitari, G., Prather, M. J., Pyle, J. A., Richter, A., Rodriguez, J. M., Savage, N. H., Strahan, S.  
25 E., Sudo, K., Szopa, S. and Van Roozendaal, M.: Multi-model ensemble simulations of  
26 tropospheric NO<sub>2</sub> compared with GOME retrievals for the year 2000, *Atmos. Chem. Phys.*,  
27 doi:10.5194/acp-6-2943-2006, 2006.  
28  
29 Vukovich, J., & Pierce, T.: The implementation of BEIS3 within the SMOKE modeling framework,  
30 in: *Proceedings of the 11th International Emissions Inventory Conference*, Atlanta, Georgia, 15  
31 April 2002, 15-18, 2002.  
32  
33 Walters, W. W., Goodwin, S. R. and Michalski, G.: Nitrogen stable isotope composition ( $\delta^{15}\text{N}$ )  
34 of vehicle-emitted NO<sub>x</sub>, *Environ. Sci. Technol.*, doi:10.1021/es505580v, 2015a.  
35  
36 Walters, W. W., Tharp, B. D., Fang, H., Kozak, B. J. and Michalski, G.: Nitrogen Isotope  
37 Composition of Thermally Produced NO<sub>x</sub> from Various Fossil-Fuel Combustion Sources,  
38 *Environ. Sci. Technol.*, doi:10.1021/acs.est.5b02769, 2015b.  
39  
40 Walters, W. W. and Michalski, G.: Theoretical calculation of nitrogen isotope equilibrium  
41 exchange fractionation factors for various NO<sub>y</sub> molecules, *Geochim. Cosmochim. Acta*,  
42 doi:10.1016/j.gca.2015.05.029, 2015.  
43  
44 Walters, W. W., Simonini, D. S. and Michalski, G.: Nitrogen isotope exchange between NO and  
45 NO<sub>2</sub> and its implications for  $\delta^{15}\text{N}$  variations in tropospheric NO<sub>x</sub> and atmospheric nitrate,  
46 *Geophys. Res. Lett.*, doi:10.1002/2015GL066438, 2016.

- 1  
2 Walters, W. W., Fang, H. and Michalski, G.: Summertime diurnal variations in the isotopic  
3 composition of atmospheric nitrogen dioxide at a small midwestern United States city, *Atmos.*  
4 *Environ.*, doi:10.1016/j.atmosenv.2018.01.047, 2018.
- 5  
6 Weber, P. and Rennenberg, H.: Dependency of nitrogen dioxide (NO<sub>2</sub>) fluxes to wheat (*Triticum*  
7 *aestivum* L.) leaves from NO<sub>2</sub> concentration, light intensity, temperature and relative humidity  
8 determined from controlled dynamic chamber experiments, *Atmos. Environ.*, doi:10.1016/1352-  
9 2310(96)00008-8, 1996.
- 10  
11 Wong, S., Wang, W. C., Isaksen, I. S. A., Berntsen, T. K. and Sundet, J. K.: A global climate-  
12 chemistry model study of present-day tropospheric chemistry and radiative forcing from changes  
13 in tropospheric O<sub>3</sub> since the preindustrial period, *J. Geophys. Res. D Atmos.*,  
14 doi:10.1029/2003JD003998, 2004.
- 15  
16 Xing, J., Pleim, J., Mathur, R., Pouliot, G., Hogrefe, C., Gan, C. M. and Wei, C.: Historical  
17 gaseous and primary aerosol emissions in the United States from 1990 to 2010, *Atmos. Chem.*  
18 *Phys.*, doi:10.5194/acp-13-7531-2013, 2013.
- 19  
20 Yan, X., Ohara, T. and Akimoto, H.: Statistical modeling of global soil NO<sub>x</sub> emissions, *Global*  
21 *Biogeochem. Cycles*, doi:10.1029/2004GB002276, 2005.
- 22  
23 Yienger, J. J. and Levy, H.: Empirical model of global soil-biogenic NO<sub>x</sub> emissions, *J. Geophys.*  
24 *Res.*, doi:10.1029/95jd00370, 1995.
- 25  
26 Yu, Z. and Elliott, E. M.: Novel Method for Nitrogen Isotopic Analysis of Soil-Emitted Nitric  
27 Oxide, *Environ. Sci. Technol.*, doi:10.1021/acs.est.7b00592, 2017.
- 28  
29 Zörner, J., Penning de Vries, M. J. M., Beirle, S., Sihler, H., Veres, P. R., Williams, J. and  
30 Wagner, T.: Multi-satellite sensor study on precipitation-induced emission pulses of NO<sub>x</sub> from  
31 soils in semi-arid ecosystems, *Atmos. Chem. Phys. Discuss.*, doi:10.5194/acp-2016-93, 2016.